# Cellular crosstalk promotes hepatic progenitor cell proliferation and stellate cell activation in 3D co-culture

Haaker, M.W.; Chang, J.C.; Chung, B.K.; Pieper, T.S.; Noé, F.; Wang, T.T.; ... ; Helms, J.B.

cmgh
CELLULAR AND MOLECULAR GASTROENTEROLOGY AND HEPATOLOGY

ORIGINAL RESEARCH

# Cellular Crosstalk Promotes Hepatic Progenitor Cell Proliferation and Stellate Cell Activation in 3D Co-culture

Maya W. Haaker,[1] Jung-Chin Chang,[1] Brian K. Chung,[2,3,4] Tobias S. Pieper,[1] Falko Noé,[5] Tongtong Wang,[5] Niels Geijsen,[6] Martin Houweling,[1] Christian Wolfrum,[5] Arie B. Vaandrager,[1] Espen Melum,[2,3,4,8,9] Bart Spee,[7] and J. Bernd Helms[1]

*[1]Department of Biomolecular Health Sciences, Faculty of Veterinary Medicine, Utrecht University, The Netherlands; [2]Norwegian PSC Research Center, Department of Transplantation Medicine, Division of Surgery and Specialized Medicine, eDivision of Surgery and Specialized Medicine, Oslo University Hospital Rikshospitalet, Oslo, Norway; [3]Institute of Clinical Medicine, Faculty of Medicine, University of Oslo, Oslo, Norway; [4]Research Institute of Internal Medicine, Oslo University Hospital, Rikshospitalet, Oslo, Norway; [5]Institute of Food, Nutrition and Health, ETH Zurich, Schwerzenbach, Switzerland; [6]Department of Anatomy and Embryology, Leiden University Medical Center, Leiden, The Netherlands; [7]Department of Clinical Sciences, Faculty of Veterinary Medicine, Utrecht University, Utrecht, The Netherlands; [8]Section of Gastroenterology, Department of Transplantation Medicine, Division of Surgery and Specialized Medicine, Oslo University Hospital Rikshospitalet, Oslo, Norway; and [9]Hybrid Technology Hub-Centre of Excellence, Institute of Basic Medical Sciences, Faculty of Medicine, University of Oslo, Oslo, Norway*

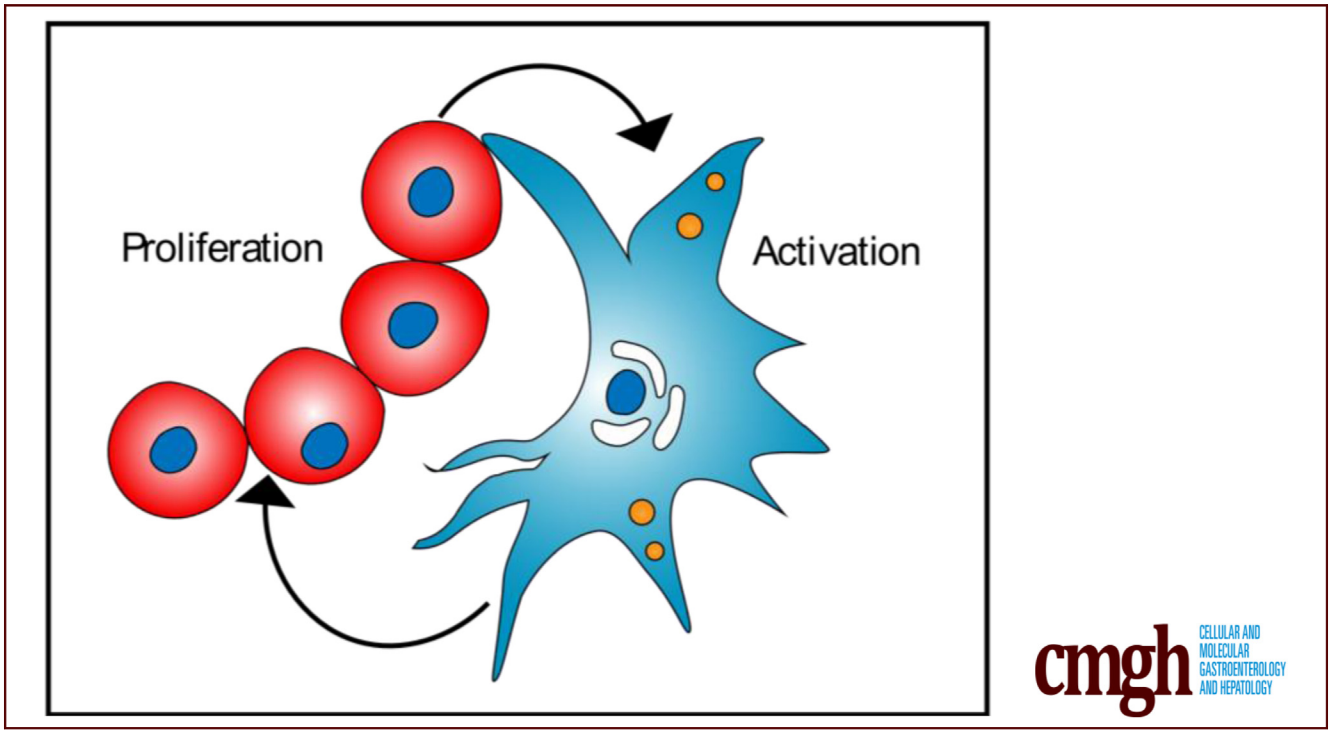


**SUMMARY**

Enhanced hepatic progenitor cell proliferation and stellate cell activation, as observed in ductular reaction with liver fibrosis, can be mimicked in an *in vitro* 3D co-culture. This provides a novel approach to elucidate the cellular interactions in liver diseases.

**BACKGROUND & AIMS:** Following liver damage, ductular reaction often coincides with liver fibrosis. Proliferation of hepatic progenitor cells is observed in ductular reaction, whereas activated hepatic stellate cells (HSCs) are the main drivers of liver fibrosis. These observations may suggest a functional interaction between these 2 cell types. Here, we report on an *in vitro* co-culture system to examine these interactions and validate their co-expression in human liver explants.

**METHODS:** In a 3D organoid co-culture system, we combined freshly isolated quiescent mouse HSCs and fluorescently labeled progenitor cells (undifferentiated intrahepatic cholangiocyte organoids), permitting real-time observation of cell morphology and behavior. After 7 days, cells were sorted based on the fluorescent label and analyzed for changes in gene expression.

**RESULTS:** In the 3D co-culture system, the proliferation of progenitor cells is enhanced, and HSCs are activated, recapitulating the cellular events observed in the patient liver. Both effects in 3D co-culture require close contact between the 2 different cell types. HSC activation during 3D co-culture differs from quiescent (3D mono-cultured) HSCs and activated HSCs on plastic (2D mono-culture). Upregulation of a cluster of genes containing *Aldh1a2*, *Cthrc1*, and several genes related to frizzled binding/Wnt signaling were exclusively observed in 3D co-cultured HSCs. The localized co-expression of specific genes was confirmed by spatial transcriptomics in human liver explants.

**CONCLUSION:** An *in vitro* 3D co-culture system provides evidence for direct interactions between HSCs and progenitor cells, which are sufficient to drive responses that are similar to those seen during ductular reaction and fibrosis. This model paves the way for further research into the cellular basis of liver pathology. *(Cell Mol Gastroenterol Hepatol 2025;19:101472; https://doi.org/10.1016/j.jcmgh.2025.101472)*

*Keywords:* Ductular Reaction; Intrahepatic Cholangiocyte Organoid; Liver Fibrosis; Retinoic Acid.

Approximately 2 million people worldwide die of liver diseases each year. The causes of chronic liver diseases include viral infection leading to hepatitis, excessive alcohol consumption or metabolic deficiencies leading to steatotic liver disease, or defects in the production and secretion of bile or bile duct inflammation leading to biliary diseases.[1] In chronic liver diseases such as metabolic dysfunction-associated steatotic liver disease (MASLD), previously known as non-alcoholic fatty liver disease (NAFLD),[2] ductular reaction is commonly observed.[3,4] Ductular reaction is a ductular phenotype[5] that has classically been described in biliary disorders. Histologically, ductular reaction can be recognized by bile duct proliferation or hyperplasia. The cellular source differs, depending on the type of liver injury, but ductular reaction may originate from: (1) pre-existing cholangiocytes; (2) transdifferentiation of hepatocytes to cholangiocytes; or (3) hepatic progenitor cells around bile ducts that are able to differentiate towards cholangiocytes and hepatocytes.[3,5] Studies on primary biliary epithelium have been limited by poor access to tissue. Organoid technology has enabled growth of cholangiocyte progenitor cells in three-dimensional (3D) culture conditions with the propagation of both intrahepatic (ICOs) and extrahepatic (ECOs) cholangiocytes from primary tissue.[6–9] Both types of cholangiocyte organoids have rather similar gene expression profiles with cholangiocyte fate differentiation capacity, but only ICOs can also differentiate to hepatocytes, suggestive of a bipotential nature.[8,10,11] Mouse ICOs (mICOs) expressed multiple progenitor cell (*Lgr5, Cd44, Sox9, Prom1, EpCAM, Foxl1, Trop2*) markers, as well as hepatocyte (*Krt8, Krt18, HNF4α Ttr*), and cholangiocyte (*Krt7, Krt19*) markers. Lineage tracing demonstrated that the ICO-initiating cells are in fact derived from adult intrahepatic cholangiocytes that undergo Tet1-mediated epigenetic reprogramming to assume a stem/progenitor cell state, both *in vitro* and *in vivo*.[11] The expansion of Lgr5$^+$ liver stem cells is induced by Wnt-driven regeneration, mediated by the leucine rich repeat containing G protein-coupled receptor 5 (LGR5) , a receptor for R-spondins.[12] By changing the growth factors in the medium, it is possible to differentiate ICOs, reducing the progenitor cell markers and increasing either hepatocyte markers or cholangiocyte markers.[13,14]

The degree of ductular reaction correlates with the severity of liver fibrosis.[15,16] When the cause for liver damage persists, liver fibrosis can develop into liver cirrhosis, which impairs liver function, and also provides a favorable environment for the development of hepatocellular carcinoma.[17] Liver fibrosis is characterized by the excessive accumulation of extracellular matrix (ECM) proteins like collagen. The main cell type producing these ECM proteins in liver fibrosis is the hepatic stellate cell (HSC).[18] HSCs in a healthy liver are quiescent, vitamin A-storing cells. Upon liver damage, they become activated, transdifferentiate into myofibroblasts, and release vitamin A, at least partially as retinoic acid (RA).[19] Classical markers of HSC activation include downregulation of lecithin:retinol acyltransferase (*Lrat*) and glial fibrillary acidic protein (*Gfap*), as well as upregulation of collagen and alpha-smooth muscle actin (*Acta2*) expression.[20] *In vitro* activation of HSCs by 2D culture on plastic surfaces mimics most of these characteristics, but some differences have been observed.[21] *In vivo,* there is also a certain level of variation. Differences in gene expression in activated HSCs exist depending on the type of liver damage,[21] and single-cell RNA sequencing has revealed heterogenicity among activated HSCs, with differences in the level of classical activation markers in the identified clusters.[22,23]

***Abbreviations used in this paper:*** **AAF, N-2-acetylaminofluorene; Acta2, alpha-smooth muscle actin; Aldh1a2, aldehyde dehydrogenase family 1, subfamily A2; ANOVA, analysis of variance; aPF, activated portal fibroblast; Apln, apelin; BDL, bile duct ligation; BSA, bovine serum albumin; CCl4, carbon tetrachloride; Col1a1, collagen 1a1; Cthrc1, collagen triple helix repeat containing-1; DDC, 3,5-diethoxycarbonyl-1,4-dihydrocollidine; DEG, differentially expressed gene; DMEM, Dulbecco's Modified Eagle Medium; ECM, extracellular matrix; ECO, extrahepatic cholangiocyte organoid; ELISA, enzyme-linked immunosorbent assay; EM, expansion medium; FACS, fluorescence-activated cell sorting; FBS, fetal bovine serum; Gfap, glial fibrillary acidic protein; GO, Gene Ontology; Gpc3, glypican 3; GSEA, gene set enrichment analysis; HSC, hepatic stellate cell; ICO, intrahepatic cholangiocyte organoid; LGR5, leucine rich repeat containing G protein-coupled receptor 5; Lrat, lecithin:retinol acyltransferase; MASLD, metabolic dysfunction-associated steatotic liver disease; MICO, mouse intrahepatic cholangiocyte organoid; Mmp7, matrix metallopeptidase 7; NAFLD, non-alcoholic fatty liver disease; NF-κB, nuclear factor-kappa B; ORA, over representation analysis; PBC, primary biliary cholangitis; PBS, phosphate-buffered saline; PBST, phosphate-buffered saline with Tween; PCA, principal component analysis; PF, portal fibroblast; PINP, procollagen type I N-terminal propeptide; Plk1, polo-like kinase 1; PSC, primary sclerosing cholangitis; RA, retinoic acid; RT-qPCR, real time quantitative polymerase chain reaction; TAA, thioacetamide; TGFβ1, transforming growth factor beta 1; 3D, three-dimensional.**

**Most current article**



2352-345X
https://doi.org/10.1016/j.jcmgh.2025.101472

It has been questioned whether ductular reaction and liver fibrosis are 2 separate responses to liver injury or if they drive each other.[24] If the 2 responses drive each other, it can be questioned which cell type initiates the reaction and whether this would then involve direct interactions between the cells.[24,25] Studies in rodent models suggest that HSC activation and collagen deposition precedes[26] or is required[27] for progenitor cell proliferation, whereas another study finds that liver fibrosis is induced via a nuclear factor-kappa B (NF-$\kappa$B)-inducing kinase/cholangiokine/HSC axis in several mice models for ductular reaction, suggesting proliferating cholangiocytes initiate the response.[28]

Investigating interactions between cell types in an animal model is complicated by the many additional factors being present, such as the other cell types in close vicinity that may also respond to liver damage. To better understand the correlation between ductular reaction and liver fibrosis, we questioned whether ICOs, as hepatic progenitor cells, and HSCs can directly communicate with each other. Three-D cultures are more representative for the native tissue as it allows the cells to grow and migrate in all directions. Therefore, we co-cultured ICOs and freshly isolated (quiescent) mouse HSCs in 3D conditions using a hydrogel generated from solubilized basement membrane matrix (ie, Matrigel). These hydrogels have been shown to prevent HSC activation,[29,30] whereas stiffer matrixes including plastic can activate HSCs.[31] We found that ICOs and HSCs in 3D co-culture directly influence each other, resulting in increased proliferation of ICOs and activation of HSCs. The interaction depends on close contact between the 2 cell types.

# Results

## HSCs in 3D Mono-culture Remain Quiescent but can be Activated by TGF$\beta$1

HSCs 3D-cultured in Matrigel remain quiescent in Dulbecco's Modified Eagle Medium (DMEM) with 10% (v/v) fetal bovine serum (FBS), whereas HSCs 2D-cultured on a plastic surface become activated. We first assessed whether isolated HSCs behave similarly in co-culture medium, consisting of 50% ICO culture medium (expansion medium) and 50% HSC culture medium (DMEM with 10% FBS). Freshly isolated quiescent HSCs were cultured in Matrigel (HSC 3D mono-culture) or plated on plastic (HSC 2D mono-culture) and cultured in co-culture medium. After 7 days of culture, HSC 3D mono-cultures had high expression of *Lrat*, a quiescence marker,[32] whereas the expression level of activation marker *Acta2*[32] was low (Figure 1*A*). HSC 2D mono-cultures gave the opposite results with low *Lrat* expression and high *Acta2* expression (Figure 1*A*). The secretion of type I collagen in the medium was also lower in HSC 3D mono-cultures as compared with HSC 2D mono-cultures. Together, these results strongly suggest that HSCs remain quiescent in Matrigel and become activated on plastic surfaces. Addition of transforming growth factor beta 1 (TGF$\beta$1), a factor involved in the HSC activation process, to HSC 3D mono-cultures lowered *Lrat* expression and increased *Acta2* and *Col1a1* expression. HSCs with TGF$\beta$1 also secreted more collagen type 1 compared with non-treated cultures (Figure 1*B*). These results indicate that quiescent HSC 3D mono-cultures can be activated by a proper stimulus like TGF$\beta$1. It is also noticeable that whereas HSC culture in 2D leads to a pronounced increase in *Acta2*, HSC activation in 3D Matrigel culture via TGF$\beta$ gave a more pronounced increase in *Col1a1* with moderately increased *Acta2*.

## Co-culture of HSCs and ICOs

We next analyzed the interaction between HSCs and ICOs by 3D co-culturing these cells in Matrigel for 7 days. We observed clear morphologic changes in both cell types during 3D co-culture as compared with 3D mono-cultures of the individual cell types under the same conditions (Figure 2). ICOs increased in size faster than mono-cultured controls. The measured increase in metabolic activity under these conditions was consistent with higher proliferation in co-culture (Figure 2*B*). HSCs in 3D mono-cultures remained small and contained large lipid droplets filled with vitamin A (as retinyl ester), which are autofluorescent (Figure 2*C*). In 3D co-culture, HSCs that were in close proximity to ICOs became elongated, with a reduced autofluorescent signal. Secretion of type I collagen increased in 3D co-cultures as compared with 2D mono-cultures of HSCs (Figure 2*D*).

To obtain in-depth understanding of the effect which the 2 cell types have on each other, we performed RNA sequence analysis on both cell types before and after mono- and co-culture in Matrigel and compared differences in gene expression. Before RNA isolation, the cell types were sorted by fluorescence-activated cell sorting (FACS) based on tdTomato-positive (ICOs) vs tdTomato-negative (HSCs) (Figure 3). For reference, samples were also taken from freshly isolated quiescent HSCs (day 0), and of 2D mono-cultured HSCs (day 7). The heatmap and the principal component analysis (PCA) of the cultured samples shows that major differences can be found between the different HSC sample groups, with 3D co-cultured HSCs moving from 3D mono-cultured HSCs towards the 2D mono-cultured HSCs. Differences between mono-cultured and co-cultured ICOs are more subtle than the differences between the HSC groups. As both cell types change their gene expression profile in co-culture, our results indicate an interaction between HSCs and ICOs.

## Co-culture With HSCs Enhances ICO Proliferation

To assess the effect of cell-cell interactions, the differentially expressed genes in ICOs due to co-culture were analyzed. The top 75 differentially expressed genes (DEGs) are depicted in a heatmap (Figure 4*A*; Supplementary Table 2). Two of the most upregulated genes in ICOs by co-culture with HSCs were matrix metallopeptidase 7 (*Mmp7*) and Glypican 3 (*Gpc3*) (Figure 4*A and E*; Supplementary Tables 2 and 3). *Mmp7* has been found upregulated in proliferating progenitor cells,[33] whereas *Gpc3* has been described as a marker for liver progenitor cells[34] and hepatocellular carcinoma.[35] Overrepresentation

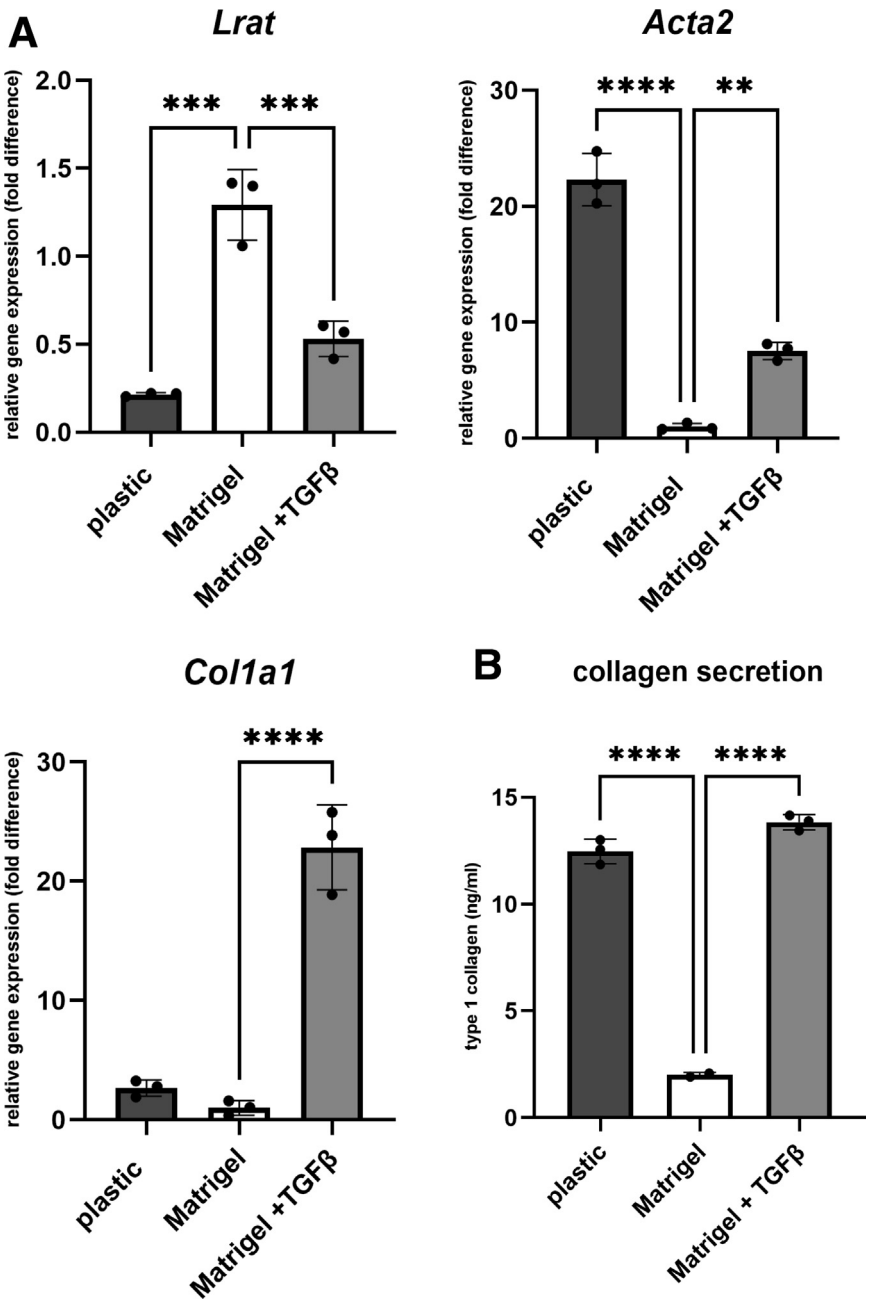


**Figure 1. Activation of HSCs in mono-culture.** Freshly isolated HSCs were cultured on plastic or in Matrigel (±10 ng/mL TGF$\beta$1) for 7 days in co-culture medium. (*A*) Cells were harvested for RNA isolation with subsequent rt-qPCR on *Lrat*, *Acta2*, and *Col1a1* gene expression. (*B*) Medium was collected and secretion of type I collagen was analyzed by ELISA. Cells were cultured in triplicate. Gene expression results were repeated for 5 different cell isolations. Data shown are from a representative experiment. *$P < .05$; **$P < .01$; ***$P < .001$; ****$P < .0001$

analysis shows that many of the DEGs are associated with cell division (Figure 4*B*). These results are consistent with the morphological observations that the ICOs grew faster in co-culture (Figure 2*A*), suggesting enhanced proliferation. ICOs have been shown to be able to differentiate and gain cholangiocyte or hepatocyte characteristics.[10] Although *Lgr5* showed a slight increase in co-culture (log2 ratio 0.69; $P < .001$), which was confirmed by real time quantitative polymerase chain reaction (RT-qPCR) (data not shown), there were no large overall effects on genes related to differentiation of the ICOs towards hepatocytes or cholangiocytes (Figure 4*C and D*).

## Co-culture With ICOs Induces HSC Activation

Similarly, the DEGs in HSCs due to co-culture were also analyzed. The top 75 DEGs are depicted in a heatmap (Figure 5*A*). For comparison, the expression of the same genes in HSCs directly after isolation (day 0, quiescent) and 2D mono-cultured HSCs is also shown. Three-D mono-cultured HSCs cluster closely to the day 0 HSCs, consistent with their quiescent state. Three-D co-cultured HSCs, on the other hand, have more resemblance with 2D mono-cultured HSCs. Many DEGs in co-cultured HSCs are related to wound healing and ECM organization, indicating active fibroblast function (Figure 5*B and C*). Combined with the morphologic

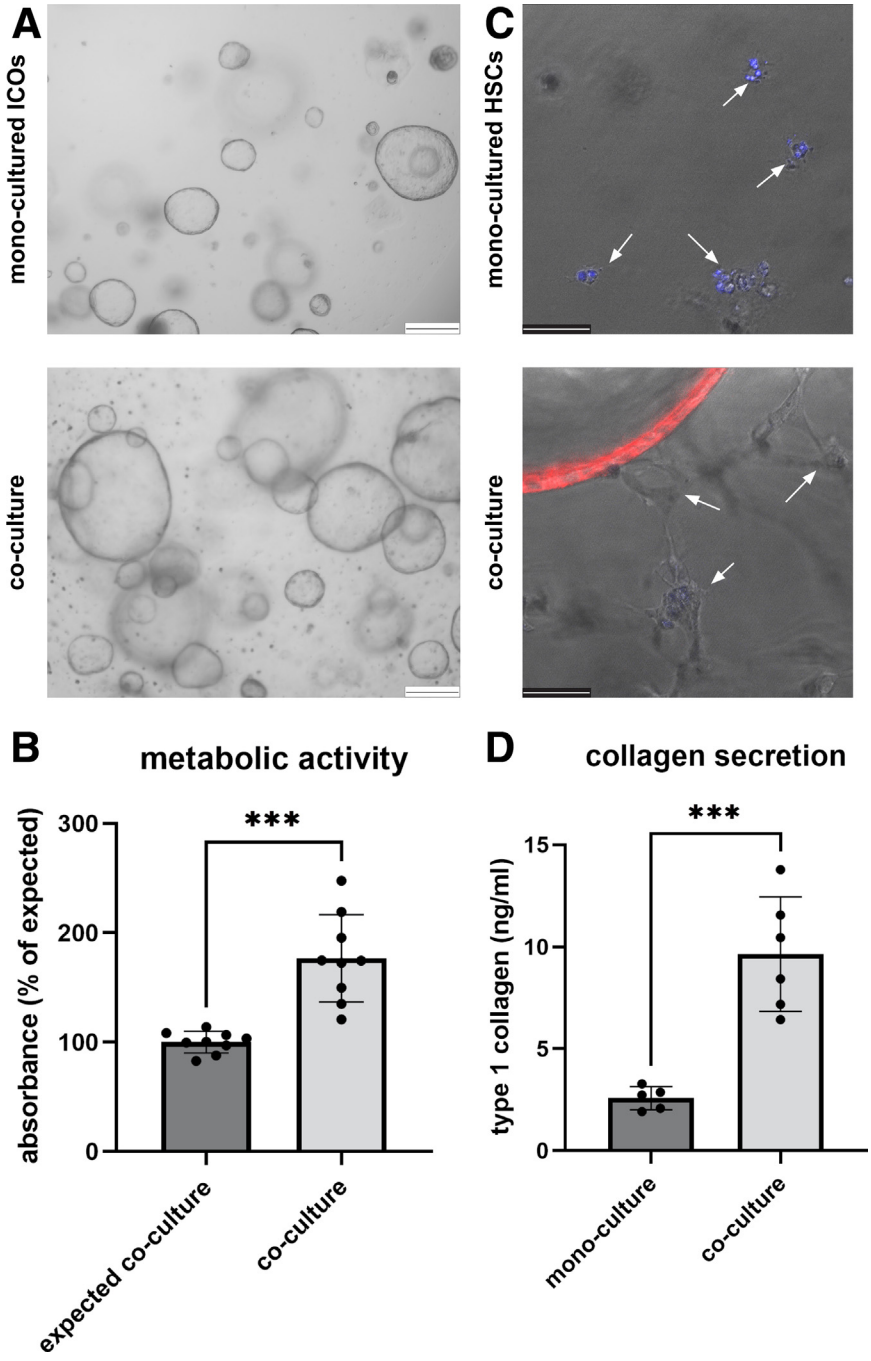


**Figure 2. ICOs and HSCs in 3D co-culture influence each other.** (*A*) Microscopy images of a 3D co-culture of HSCs and ICOs and a 3D mono-culture of ICOs after 7 days of culture. Scale bar = 400 $\mu$m. (*B*) In co-culture, one-half of the amount of HSCs and one-half of the amount of ICOs was plated as compared to their respective mono-culture. Therefore, the expected metabolic activity (when no interaction between different cell types takes place) is defined as the 0.5× (the metabolic activity of ICO 3D mono-culture + the metabolic activity of HSC 3D mono-culture). The signal measured in the 3D co-culture was significantly ($P < .001$) higher. (*C*) Confocal images of 3D mono- and 3D co-cultured HSCs in Matrigel. *Blue* = autofluorescence from retinyl esters; *red* = tdTomato from ICOs; *arrows* indicate HSCs. Scale bar = 36.6 $\mu$m. (*D*) Type 1 collagen secretion of 3D mono HSC culture vs 3D co-culture, data collected from 2 different experiments performed in triplicate. *$P < .05$; **$P < .01$; ***$P < .001$; ****$P < .0001$

changes and increase in type 1 collagen secretion as shown in Figure 2, these data indicate activation of HSCs due to co-culture with ICOs. Indeed, the classic HSC activation markers *Acta2* and *Col1a1* are both upregulated in 3D co-cultured HSCs and 2D mono-cultured HSCs (which we will refer to from here on as co-culture- vs plastic-activated HSCs). *Col1a1* was more pronounced in co-culture-activated HSCs than in plastic-activated HSCs, whereas *Acta2* was more pronounced in plastic-activated HSCs (Figure 5*D*). Interestingly, this trend is similar to the activation of 3D mono-cultured HSCs by TGF$\beta$1 (Figure 1).

There are also some differences in gene expression between co-culture-activated HSCs and plastic-activated HSCs (Figure 5*A*). Overrepresentation analysis of these DEGs contains Gene Ontology (GO) terms like ECM organization, actin filament organization, and cell adhesion (Figure 5*E–J*). Many types of collagen (as markers for HSC activation) are upregulated in plastic and /or co-culture activation, as demonstrated by an increase in *Col3a1*, *Col12a1*, and *Col1a1* expression (Figure 5*D*). Some genes are specifically upregulated in co-culture-activated HSCs only as compared with all other conditions of HSC culture (Figure 5*A and D*; see

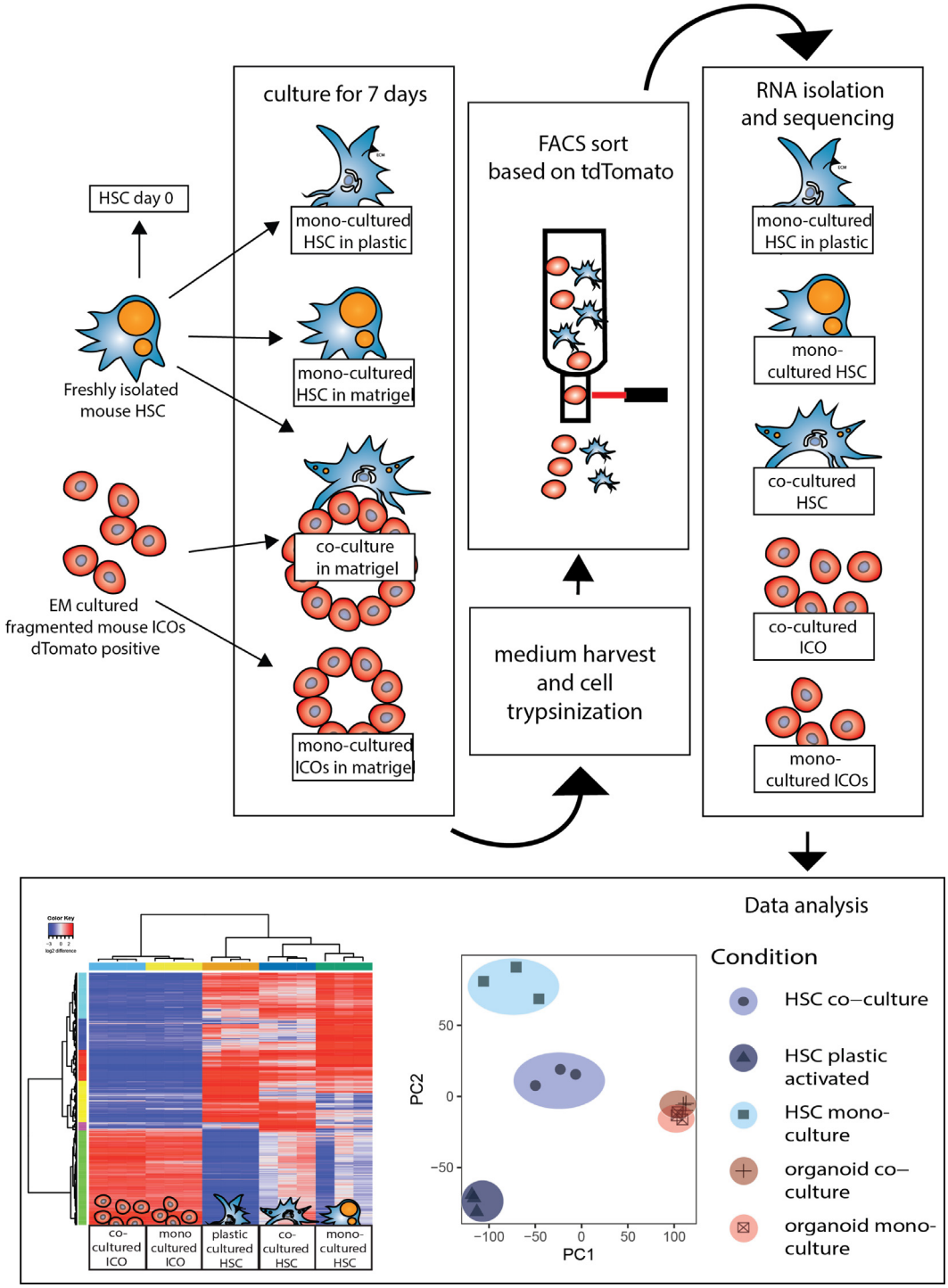


**Figure 3. Workflow of RNA sequence analysis in co-culture experiments.** HSCs were freshly isolated from healthy mice, a day 0 sample was taken. tdTomato-positive mouse ICOs from EM culture conditions were fragmented. Both cell types were cultured for 7 days under various conditions as shown, with medium refreshed every 3 days. Cells were harvested and trypsinized to obtain single cells, after which the cells were sorted based on the tdTomato signal in the ICOs. Mono-cultures were taken through the same sorting procedure. Bulk RNA was isolated and sequenced. Data analysis panel shows a heatmap of differential gene expression (Log2 fold change of normalized counts) and the PCA for gene expression of both mono- and co-cultured HSCs and ICOs.

also Figure 3 magenta cluster). A list of the magenta cluster (Figure 3) representing the specifically upregulated genes in co-culture activated HSCs is presented in Supplementary Table 4.

### *Specifically Upregulated Genes in Co-cultured HSCs: Involvement of RA and Wnt*

The specific upregulation of aldehyde dehydrogenase family 1, subfamily A2 (*Aldh1a2*, also known as retinaldehyde

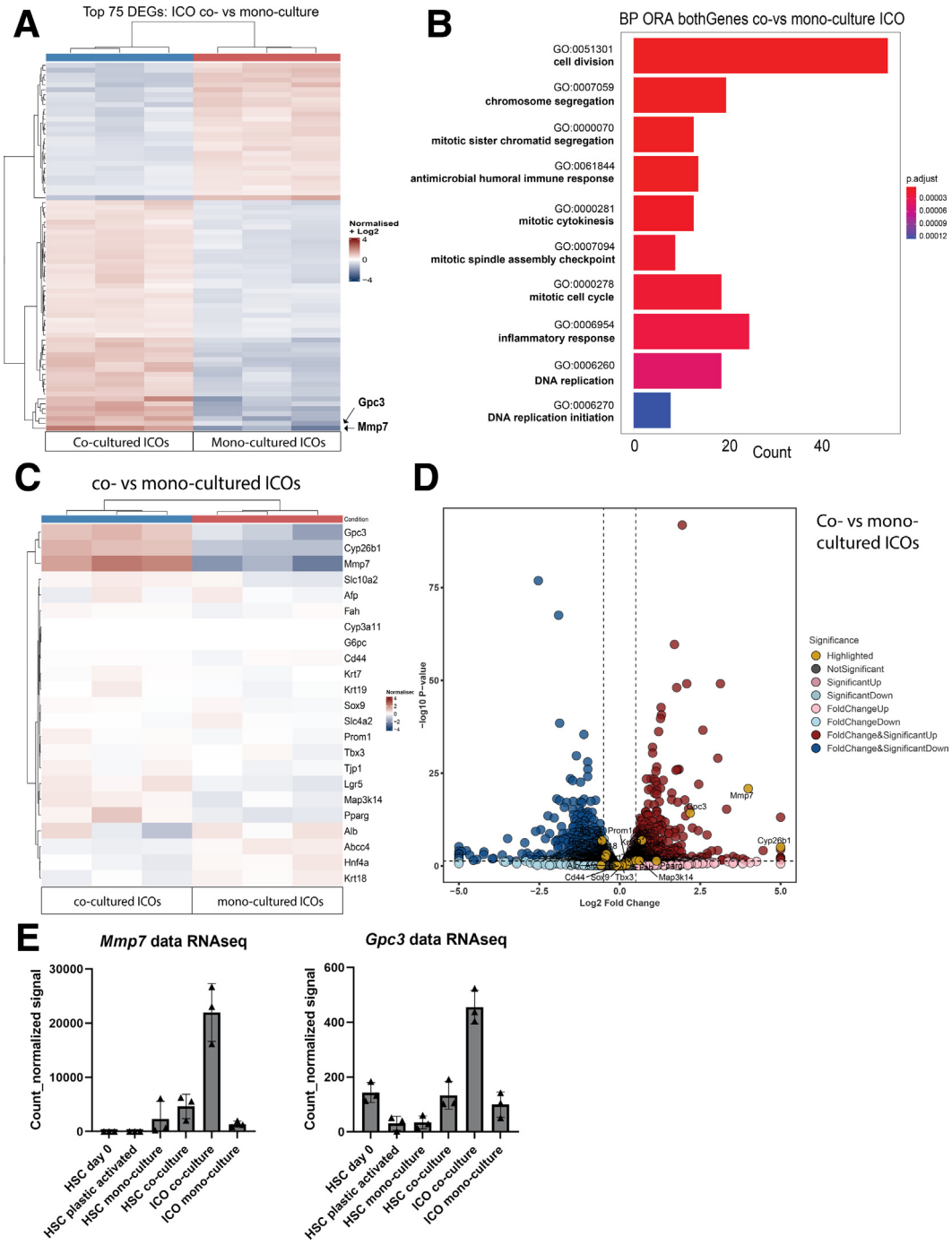


**Figure 4. Changes in gene expression of ICOs during co-culture.** (*A*) Heatmap of the top 75 DEGs comparing co-cultured ICOs with mono-cultured ICOs. (*B*) ORA of biological processes (BP) related to DEGs in co-cultured vs mono-cultured ICOs. (*C*) Heatmap of a selection of genes related to differentiation of progenitor state of ICOs. Also included are 3 genes (*Gpc3*, *Mmp7*, *Cyp261b*) from the top DEGs to show contrast. (*D*) Same genes from *A* shown in a volcano plot. (*E*) Bar charts from the RNA sequencing normalized counts for *Mmp7* and *Gpc3* expression over all samples.

dehydrogenase 2) in co-cultured HSCs vs plastic-activated HSCs (Figure 5*D*) was verified by rt-qPCR after sorting of the cells (Figure 5*G*). *Aldh1a2* encodes for an enzyme producing RA, a metabolite of vitamin A, which is thought to be synthesized by HSCs during HSC activation.[36] To investigate the possibility that production of retinoic acid might play a role in the signaling between the 2 cell types, all-trans-RA was added to ICO mono-cultures. This did not affect their proliferation (Figure 6*A*) but increased the expression of a subset of genes which were also induced in ICOs by co-culture with HSCs. All-trans-RA upregulated the expression of *Mmp7* and *Gpc3* (Figure 6*B and C*), whereas gene expression of Polo-like kinase 1 (*Plk1*) (related to proliferation, and one of the DEGs related to the GO term cell division)

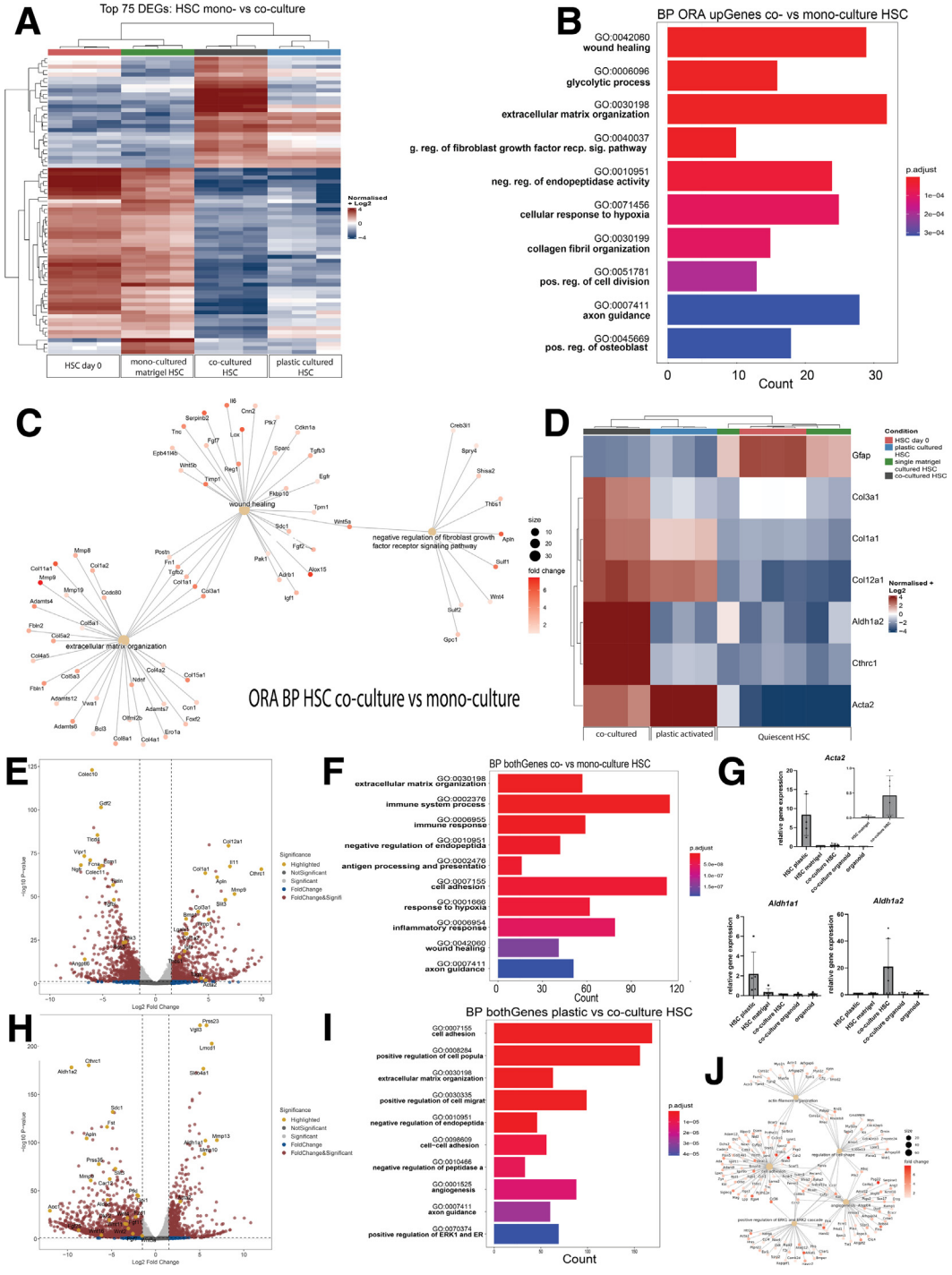


**Figure 5. Changes in gene expression of HSCs during co-culture.** (*A*) Heatmap of the top 75 DEGs in 3D mono- versus co-cultured HSCs, with the expression in HSCs directly after isolation (day 0, quiescent HSCs) and 2D mono-cultured HSCs for 7 days (activated HSCs) for comparison. (*B*) ORA of biological processes (BP) related to DEGs (upregulated) in 3D co-cultured vs 3D mono-cultured HSCs. (*C*) Dot plot of genes associated with BP from *B*. (*D*) Heatmap of genes related to activation. (*E*) Volcano plot of DEG and (*F*) BP related to DEG both up and down regulated between 3D co- vs mono-cultured HSCs. (*G*) Relative gene expression of *Aldh1a1, Aldh1a2, and Acta2*, measured with rt-qPCR from cells from 3 experiments cultured in duplicate and sorted with FACS. *Aldh1a2* expression was for each experiment highest in the co-cultured HSCs, although there was variation in the level of upregulation, varying from 2 until 45 times the amount found in 3D mono Matrigel culture. (*H*) Volcano plot comparing gene expression of plastic- vs co-culture-activated HSCs. (*I*) BP related to DEG both up and down regulated between plastic- vs co-culture-activated HSCs. (*J*) Network plot showing upregulated genes in plastic culture compared with co-cultured HSCs related to several BP shown in *I*.

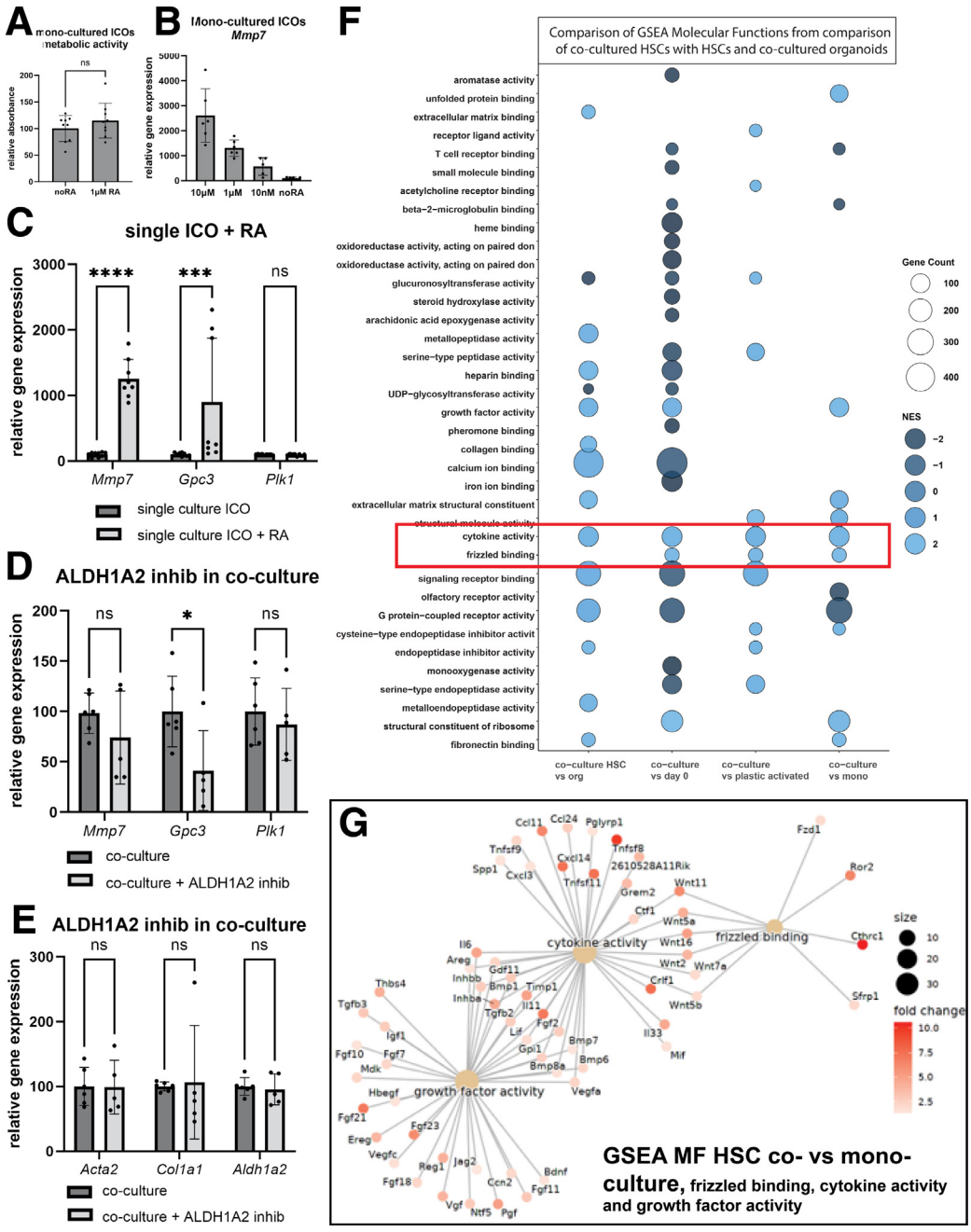


**Figure 6. Wnt and RA signaling in ICO-HSC co-cultures.** (*A*) Metabolic activity (amount of viable cells) in mono-cultured ICOs with and without RA suppletion. (*B*) Concentration range for the effect of all-trans-RA on the expression of *Mmp7* in mono-cultured ICOs. (*C*) Effect of the addition of 1 $\mu$M RA on mono-cultured ICOs on the expression of *Mmp7, Gpc3,* and *Plk1*, repeated 3 times in culture triplicate. (*D–E*) Effect of co-culture in the presence of the ALDH1A2 inhibitor WIN18,446 (2 $\mu$M) on the expression of *Mmp7, Gpc3,* and *Plk1 (D) and Acta2*, *Col1a1* and *Aldh1a2 (E)*. Data comes from 2 different mouse isolations for HSCs, cultured in triplicate. (*F*) Molecular functions (MF) identified by GSEA when comparing co-cultured HSCs with HSCs at day 0, after 7 days on plastic (2D), mono-cultured in Matrigel (3D), or co-cultured ICOs. Marked in *red* are the MFs upregulated in comparison to all other HSC conditions. (*G*) Dot plot of genes associated with MF frizzled binding, cytokine activity, and growth factor activity and found upregulated in co-cultured HSCs compared with 3D mono-cultured HSCs. *$P < .05$; **$P < .01$; ***$P < .001$; ****$P < .0001$

(Figure 4*B*) was not affected. Vice versa, treatment of co-cultures with an ALDH1A2 inhibitor (WIN18,446) led to lower levels of *Gpc3* (Figure 6*D*). These data suggest that RA production by ALDH1A2 and the subsequent secretion by the HSCs plays a role in the increase in *Gpc3* expression in the ICOs. The ALDH1A2 inhibitor did not affect gene expression of HSC-related genes (Figure 6*E*), indicating that HSC activation is not affected by the inhibitor.

Analysis on the molecular functions related to the DEGs specific in co-culture-activated HSCs and in comparison to

several other culture conditions indicated a role for the Wnt signaling pathway. As shown in Figure 5*A*, co-culture-activated HSCs show distinct changes in gene expression as compared with other culture conditions. To investigate the overall changes, we compared the gene set enrichment analysis (GSEA) of the DEG from co-cultured HSCs with those of mono-cultured HSCs (2D and 3D), HSCs (day 0) and co-cultured ICOs (Figure 6*F*). The molecular function 'cytokine activity' was increased in co-cultured HSCs as compared with all other HSC groups and also increased as compared with co-cultured ICOs. The molecular function 'frizzled binding' was also increased as compared with all other HSC groups. This molecular function relates to Wnt signaling, and our data suggest that this is specifically upregulated in co-culture-activated HSCs. As there is no overall difference in the molecular function 'frizzled binding' between co-cultured HSCs and organoids, our data suggest that both co-culture-activated HSCs and ICOs have active Wnt signaling. For ICOs, it is known that they depend on Wnt signaling to proliferate.[10] They require R-spondin (which enhances Wnt signaling) but no direct Wnt supplementation,[10,12] indicating they are actively producing Wnt. In Figure 6*G*, the DEGs between co-cultured vs mono-cultured HSCs that are related to 'cytokine activity' and 'frizzled binding' are shown. Several DEGs are related to both molecular functions ('cytokine activity' and 'frizzled binding') including several different Wnt genes. To investigate whether co-culture effects depend on Wnt signaling, we employed C59 and IWP-2, 2 general Wnt inhibitors affecting both the canonical and non-canonical Wnt signaling pathways by inhibiting porcupine, which is required for Wnt palmitoylation and secretion.[37] As mentioned above, ICOs require active Wnt signaling, and therefore, proliferation was reduced by both general Wnt inhibitors in mono-cultured as well as co-cultured ICOs, together with a strong reduction in *Mmp7* expression (Figure 7*A and B*). Addition of C59 to co-cultures deceased collagen secretion in the medium (Figure 7*C and D*). C59 did not reduce HSC-specific *Acta2* and *Col1a1* gene expression, but there was a decrease in *Aldh1a2* expression (Figure 7*E*). These data suggest that a specific part of the co-culture effects on the HSCs depends on Wnt signaling. To distinguish between different Wnt signaling pathways, we employed inhibitors that are specific of the canonical (ICG-001 and LF-3) and non-canonical (SP600125) pathways.[38–40] ICG-001 and LF-3 reduced collagen secretion, but SP600125 showed a stronger inhibitory effect by inhibiting collagen secretion, *Mmp7* expression, and proliferation of especially the co-culture (Figure 7*F–H*). However, SP600125 did not decrease *Aldh1a2* expression. Thus, inhibition of JNK as part of the non-canonical Wnt pathway seems more effective as compared with canonical Wnt inhibition, but only general Wnt inhibition (C59, IWP-2) inhibits proliferation, collagen secretion, and both *Aldh1a2* and *Mmp7* expression.

## Activation of HSCs Requires Close Contact With ICOs

To determine whether the aforementioned interactions between ICOs and HSCs in co-culture depend on close cell-cell contact or are mediated by secreted signaling molecules, cells were plated together in one droplet of Matrigel (as in previous experiments) or in separate droplets plated in the same well. Co-culture in separate droplets did not show the increase in proliferation of ICOs seen by co-culture with close contact (Figure 8*A and B*). In addition, HSCs co-cultured with ICOs in separate droplets did not display the elongated morphology as observed in HSCs co-cultured with ICOs in the same droplets, and there was no increase in collagen type 1 secretion, and gene expression of *Acta2*, *Col1a1*, and *Aldh1a2* was lower (Figure 8*A, C and D*). These results suggest that HSCs do not show signs of activation in the absence of close contact with ICOs.

## Localized Expression of Co-culture-specific Genes in Human Fibrotic Liver Assessed by Spatial Transcriptomics

To examine whether our observations that the interactions between ICOs and HSCs in co-culture depended on close cell-cell contact were relevant during liver fibrosis *in vivo*, we compared localized gene expression profiles in human fibrotic tissue from 8 patients with end-stage liver disease previously analyzed by spatial transcriptomics.[41] Of these patients, 4 suffered from primary sclerosing cholangitis (PSC), 2 from primary biliary cholangitis (PBC) and two from alcohol-related liver disease, and using these samples, it had previously been shown that parenchymal and fibrotic liver regions express unique gene content within cirrhotic liver and that the spatial transcriptomics method allows localization of gene content and cell lineages.[41] Signatures of activated HSCs (positive for *ACTA2, COL1A1, and VIM*)[41] and markers for ductular reaction and cholangiocyte progenitor cells (*KRT7, KRT19, and CD44*) were found to have higher expression in fibrotic areas as defined by spatial transcriptomics, indicating that both cell types were in proximity to each other (Figure 9*A*). Interestingly, the expression of the co-culture specific genes we had identified in HSCs (*COL1A3* and *CTHRC1*) and in ICOs (*MMP7* and *GPC3*) showed a similar degree of spatial overlap (Figure 9*B*). The expression of other co-culture specific genes (*ALDH1A2, LGR5, WNT5A, WNT11*) was below the detection limit of the method (Figure 9*C*). Clustering analysis of the differential gene content from all spatial RNA capture spots in the 8 different patients revealed 6 different clusters, with clusters 3 to 5 localizing to fibrotic areas (Figure 9*D and E*). Most of the genes of interest (mentioned above) showed highest expression within cluster 3 as compared with the other clusters (Figure 9*E*), including co-expression of the HSC (*COL3A1* and *CTHRC1*) and ICO (*GPC3* and *MMP7*) co-culture-specific markers (Figure 9*F*).

To further quantify the co-occurrence of co-culture-induced gene expression *in vivo*, correlation coefficients within spatial RNA capture spots were calculated (Figure 9*G*). As each RNA capture spot has a diameter of 50 $\mu$m and is expected to contain ~10 to 30 cells, we reasoned that a positive correlation between expression of co-culture-related genes from both cell types within the spots would

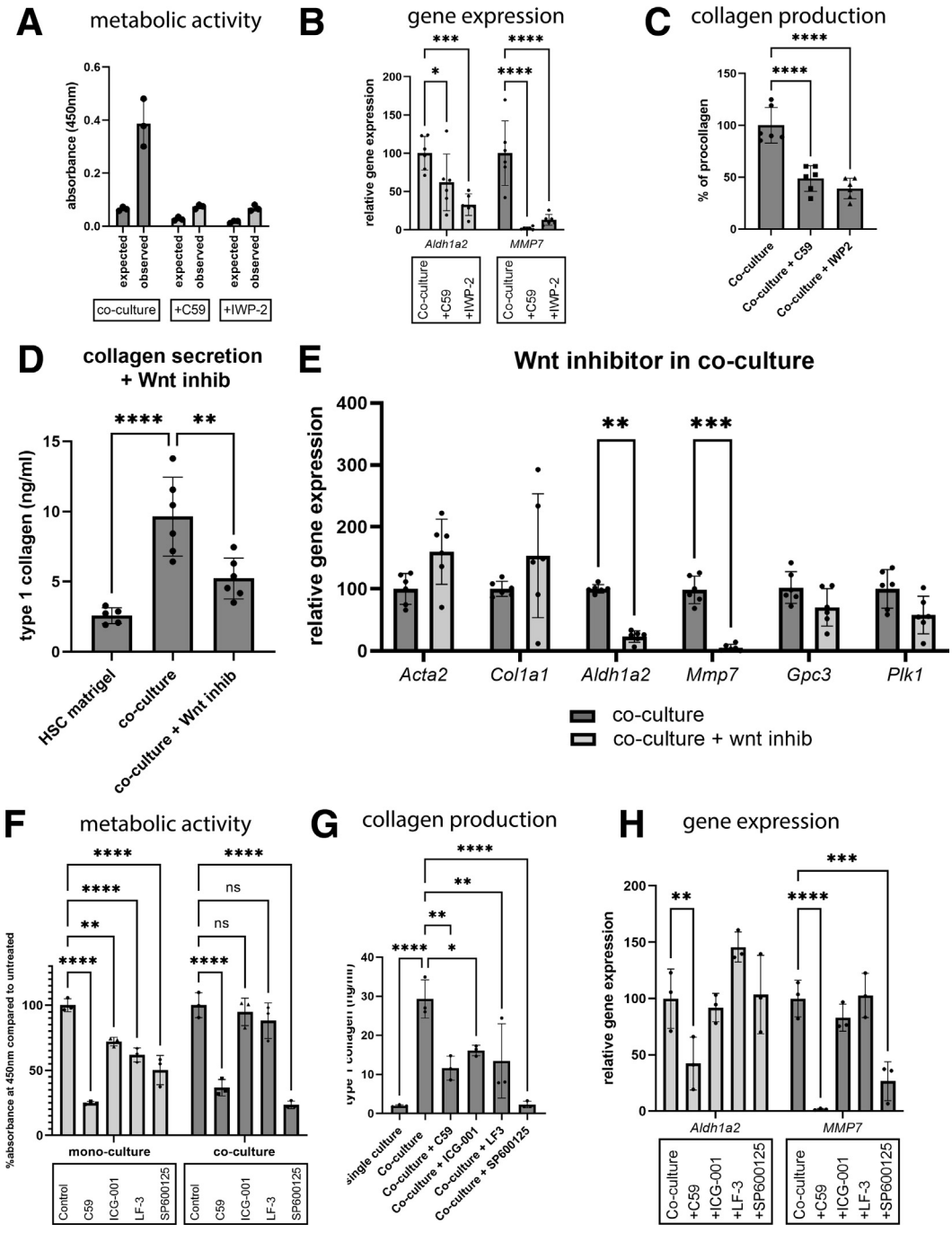


**Figure 7. Effects of Wnt inhibitors on co- vs mono-culture proliferation, collagen production, and *Aldh1a2* and *Mmp7* expression.** (*A–C*) Effect of C59 (100 nM) and IWP-2 (5 $\mu$M) on (*C*) metabolic activity, (*D*) procollagen secretion, and (*E*) relative gene expression (% compared with signal in co-culture) of *Aldh1a2* and *Mmp7* in co-culture or mono-cultured ICOs. Cells were cultured in triplicate. (*D*) Type I collagen secretion in the presence of the Wnt inhibitor C59 (100 nM) in co-culture. (*E*) Effect of co-culture in the presence of the Wnt inhibitor C59 (100 nM) on the expression of HSC-associated genes *Col1a1*, *Acta2*, and *Aldh1a2* and *Mmp7* (ICO-associated), *Gpc3* (ICO-associated) and *Plk1* (proliferation). (*F–H*) Effect of C59 (100 nM), ICG-001 (1 $\mu$M), LF-3 (5 $\mu$M), and SP600125 (10 $\mu$M) on metabolic activity, procollagen secretion, and relative gene expression. *$P < .05$; **$P < .01$; ***$P < .001$; ****$P < .0001$.

indicate that proximity is also a factor *in vivo*. Indeed, within cluster 3, the correlation coefficient for *MMP7* and *COL3A1* was R = 0.5 ($P < .0001$) (Figure 9*H*). A significant positive correlation was also found between *MMP7* and *CTHRC1* (0.26; $P < .0001$), despite a lower number of *CTHRC1*-positive spots, which negatively affected the correlation score. Within parenchymal cluster 2, where activated HSCs and ductular reaction were less present, the correlation coefficients were considerably lower (0.21 for *MMP7* with *COL3A1* and 0.08 for *MMP7* with *CTHRC1*) (Figure 9*H*).

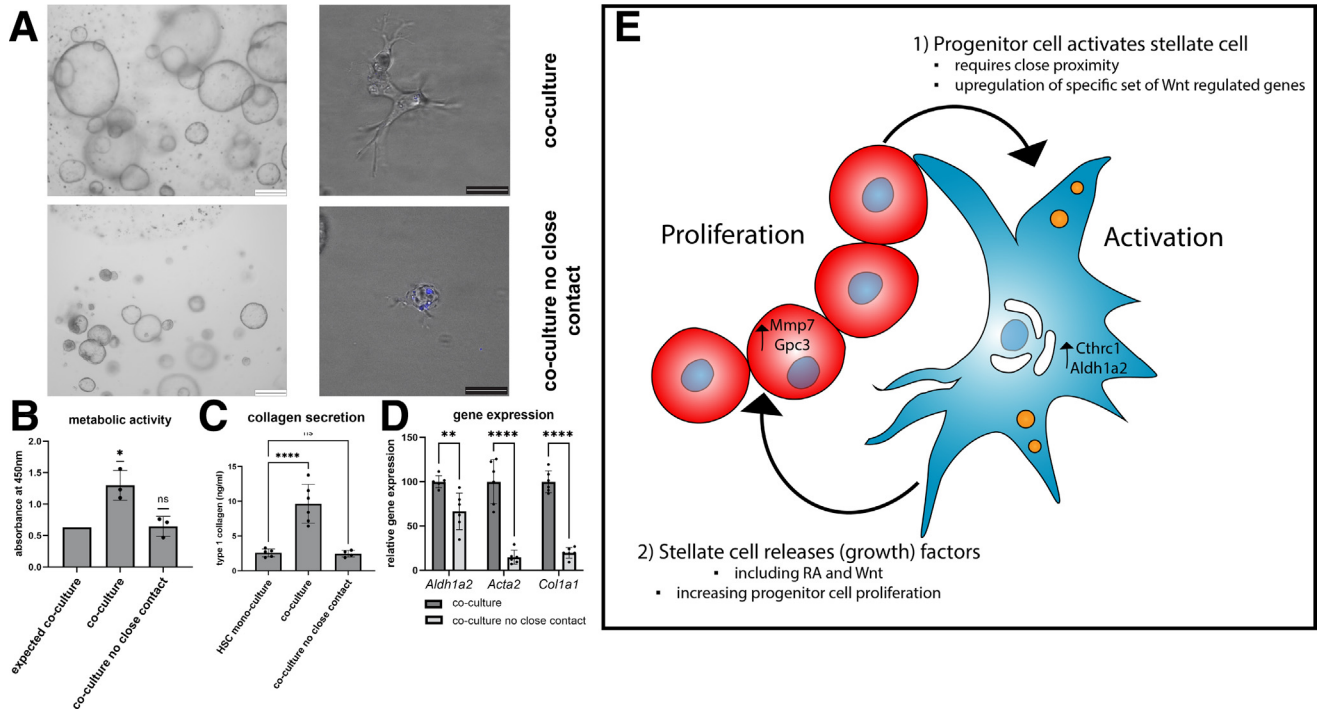


**Figure 8. HSC activation requires close contact with organoids.** (*A*) Top panels show microscopy pictures of a co-culture of ICOs (*left panel*, brightfield image) and HSCs (*right panel*, confocal microscopy) in close contact (ie, in the same Matrigel droplet). Bottom panels show the same type of images of a co-culture where HSCs and ICOs were plated without close contact (ie, in 2 separate Matrigel droplets in the same culture well). Scale bar left panels: 400 $\mu$m; right panels: 25 $\mu$m. (*B*) Metabolic activity (corresponding to cell amounts) expected based on 3D mono-cultured HSCs and ICOs, and the observed signal in co-culture with and without close contact. (*C*) Collagen type 1 secretion in the medium from HSCs in 3D mono-culture, co-culture with and without close contact. (*D*) Gene expression of HSC associated genes in co-culture with and without close contact. Data comes from 2 different mouse isolations cultured in triplicate. (*E*) Model based on the presented data, where (1) progenitor cells activate HSCs, which requires close contact, and (2) activated HSCs enhance progenitor cell proliferation. *$P < .05$; **$P < .01$; ***$P < .001$; ****$P < .0001$.

## Discussion

Here, we studied the interactions between primary quiescent HSCs and ICOs (progenitor cells) by co-culturing them in Matrigel. In many ways, effects observed in our co-culture mimic the *in vivo* situation after liver damage. Similar to liver injury with ductular reaction and liver fibrosis, co-culture of ICOs and HSCs leads to activation of the HSC and enhanced proliferation of the ICOs. In the co-culture, no additional factors (such as the presence of damaged hepatocytes) were required for HSC activation and enhanced ICO proliferation. Of note, ICOs in mono-culture under 3D conditions already actively proliferate. Whether this more closely mimics progenitor cells in a healthy liver or in a damaged liver remains to be established, but it suggests that proliferating intrahepatic cholangiocytes can induce HSC activation. *In vivo*, HSCs have been found in very close proximity to expanding progenitor cells during liver injury.[26,42] This is reflected in our ICO-HSC co-culture model, in which close proximity is essential for induction of HSC activation and enhancement of ICO proliferation. These results were also shown to be relevant *in vivo* by using spatial transcriptomics to assess fibrotic areas of human liver, demonstrating proximity of activated HSCs and cholangiocyte progenitor markers, and a correlation between expression of specific 'co-culture-related' genes. Our hypothesis is that close proximity of HSCs with ICOs is necessary for the activation of the HSCs, after which the factors excreted by the activated HSC stimulate ICO proliferation (Figure 8*E*). Future experiments will be required to establish the sequence of the events in more detail. It will also be of interest to include other cell types in the co-culture (for example, macrophages and other immune cells) to study their role in modulating the interactions between ICOs and HSCs.

The co-culture system may also contribute to the discussion on the origin of myofibroblasts in fibrotic livers. Major sources of myofibroblasts in liver fibrosis are the endogenous liver mesenchymal cells, which consists of portal fibroblasts (PFs) and HSCs. Their contribution may depend on the etiology of liver disorders and range from more than 70% by activated PFs (aPFs)[43] to HSCs being the dominant contributors to liver fibrosis.[18,44] Possibly, the interaction between cholangiocytes and aPFs in ductular reaction is more relevant at the onset of cholestatic liver injury, after which HSCs become activated and contribute more to the myofibroblast population.[43] It will be interesting to study the interaction between PFs and ICO in the co-culture system as well.

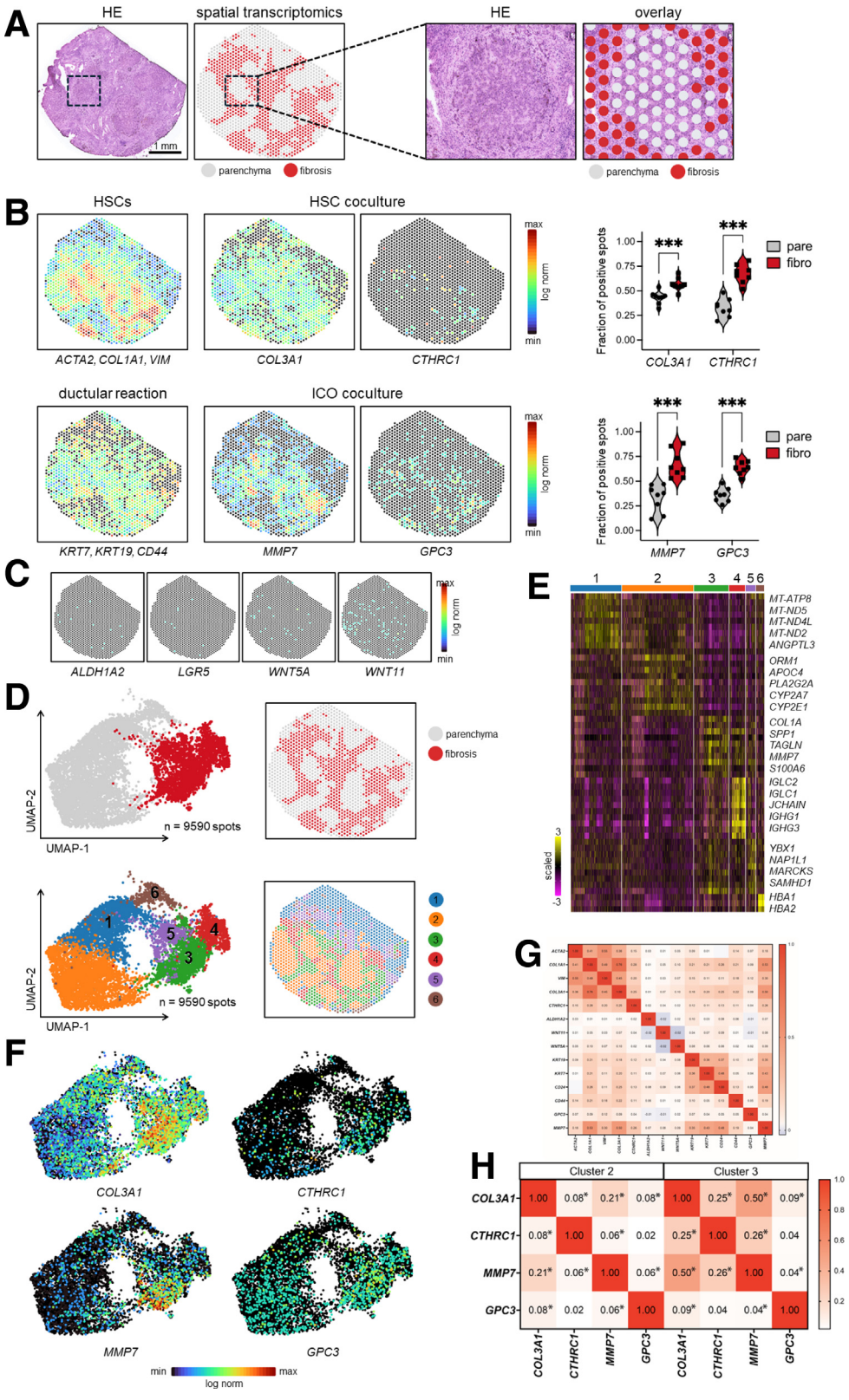


**Figure 9. Markers of HSCs and DR colocalize within fibrotic liver regions of human explants.** (*A*) Representative hematoxylin and eosin (HE) staining and spatial transcriptomics of liver sections from human liver explants. Dotted boxes indicate magnified regions. Spatial feature maps show expression of indicated genes. (*B*) Fraction of total RNA capture spots positive for indicated gene expression and located in parenchymal (pare) or fibrotic (fibro) regions as classified by spatial transcriptomics (n = 8 livers). (*C*) Spatial feature maps show expression of indicated genes. (*D*) Uniform manifold approximation and projections (UMAPs) indicate clustering analysis of differential gene content measured by spatial transcriptomics. Feature maps show spatial location of annotated clusters. (*E*) Heatmap of highly-expressed differential gene content per cluster measured by spatial transcriptomics. Rows represent genes, columns indicate RNA capture spots. Top 3 to 5 genes shown per cluster. (*F*) UMAPs showing expression of COL3A1, CTHRC1, MMP7, and GPC3 across all clusters. (*G*) Correlation matrix of genes related to HSCs or ductular reaction/progenitor cells within cluster 3. (*H*) Correlation gene expression matrix for *COL3A1, MMP7, CTHRC1,* and *GPC3* within cluster 2 vs 3. * = significant ($P < .05$).

## Co-culture Mimics the Behavior of Progenitor Cells and HSCs in Ductular Reaction In Vivo

We found that the expression of *Mmp7* and *Gpc3* is upregulated in co-cultured ICOs upon interaction with HSCs. Both genes are also upregulated in livers with ductular reaction. MMP7 is a biomarker for fibrosis in the serum of patients with MASLD,[45] and in children with a cholangiopathy that obliterates the bile ducts, leading to cholestasis and liver fibrosis called biliary atresia.[46] The serum level of MMP7 in patients with biliary atresia correlates with an increased *MMP7* gene expression in their livers. Histology analysis revealed increased ductal proliferation, and immunohistochemistry confirmed increased MMP7 in intrahepatic bile ducts.[47] In mice, treatment with thioacetamide (TAA) or 3,5-diethoxycarbonyl-1,4-dihydrocollidine (DDC) induced expression of both *Mmp7* and *Ctgf* in bile ducts.[48] Similarly, in our co-cultured ICOs, the expression of *Ctgf* is also slightly increased compared with mono-cultured ICOs (log2ratio 0.89; $P < .001$). In rats, induction of hepatic progenitor cell (oval cell) proliferation by N-2-acetylaminofluorene (AAF)/carbon tetrachloride ($CCl_4$) or partial hepatectomy also led to increased gene expression of, respectively, *Mmp7*[33] and *Gpc3*[34] in whole livers and specific immune-staining of progenitor cells. Furthermore, in hepatocellular carcinoma (and several other types of cancers), both *MMP7* and *GPC3* are upregulated and associated with increased proliferation.[49–53] We showed relevance of our co-culture model system *in vivo* by reanalyzing a spatial transcriptomics dataset in human fibrotic tissue from 8 different patients. We showed a significant enrichment of the co-culture specific expression of HSC genes (*COL3A1* and *CTHRC1*) and ICO genes (*MMP7* and *GPC3*) in fibrotic areas of the liver. In addition, we showed a significant correlation between *COL3A1* and *MMP7* in single RNA capture spots. The validation of expression of several other co-culture-specific genes (*ALDH1A2, LGR5, WNT5A, WNT11*) could not be performed by spatial transcriptomics due to low expression levels. Several other previously reported factors further support the validation of our system. We observed that HSCs in co-culture decrease expression of Gdf2/BMP9. BMP9 is mainly produced by HSCs in the liver[54] and shows an initial decrease following liver injury, which enhances liver regeneration and ductular reaction.[54,55] Apelin (*Apln*), which was upregulated in HSCs in our co-culture model, has also been shown to increase cholangiocyte proliferation and HSC activation, and *Apelin*$^{-/-}$ mice had reduced cholangiocyte proliferation and fibrosis after bile duct ligation (BDL).[56]

In our ICO-HSC coculture model, HSCs co-cultured in Matrigel with ICOs showed key hallmarks of activation, including enlarged cell size with cellular protrusions, increased secretion of type I collagen, and elevated *Acta2* expression compared with quiescent HSCs. Several genes related to wound healing and ECM organization (including multiple types of collagen, *Mmp9*, and *Timp1*) are increased in expression in co-cultured HSCs. Interestingly, *Mmp9* and *Timp1* are also upregulated in HSCs exposed to cholangiokines.[28] MMP7, which is upregulated in co-cultured ICOs, is a matrix metalloproteinase that not only remodels the ECM (eg, collagen type IV, laminin, and elastin)[46,57] but also activates pro-MMP9 by proteolytic cleavage.[58] Thus, remodeling of the ECM represents an important functional outcome and a possible mechanism of HSC-ICO interactions.

## Differences Between Plastic or Co-culture Activation of HSCs

Differences between plastic culture activation and *in vivo* activation have been observed before.[21] Culturing HSCs in soft gel may be physiologically more relevant and closer to the *in vivo* situation. Indeed, HSCs remain quiescent in the absence of external stimuli (Figure 1). Activation of HSCs in Matrigel by either TGF$\beta$1 or co-culture with ICOs induces the gene expression of the ECM protein *Col1a1* more than the expression of *Acta2*, as compared with plastic activation of HSCs. Direct comparison between activation in Matrigel and *in vivo* activation is still lacking, but analysis of HSC activation in co-culture shows some intriguing differences with HSC activation on plastic. Several genes are specifically upregulated, including *Cthrc1*, *Aldh1a2*, *Mmp9, Col3a1,* and *Apln*.

Collagen triple helix repeat containing-1 (CTHRC1) has been shown to induce low-grade activation of TGF$\beta$ signaling in adipose tissue,[59] and to be upregulated specifically in fibrosis-related fibroblasts in lung and cardiac fibrosis.[60,61] It was hardly induced in plastic-activated HSCs but upregulated in HSCs from BDL- or $CCL_4$-treated livers.[21] CTHRC1 was found to form an autocrine loop in activating HSCs, enhancing TGF$\beta$ signaling and non-canonical Wnt, with the Wnt signaling enhancing migration and contractility.[62]

Upregulation of *Aldh1a2* in co-culture activated HSCs suggests an involvement of RA in the interaction between HSCs and ICOs. Quiescent HSCs store around 80% of the vitamin A in the body.[63] These stores are reduced during HSC activation[64] and liver regeneration, where lack of retinoid stores reduces the initial regeneration response.[65] RA is an active metabolite of vitamin A that can bind nuclear receptors. The activation of HSCs by ICOs in combination with the significant increase in *Aldh1a2* expression suggests that part of the stored retinol/vitamin A is used to produce RA. At the receiving end, ICOs in co-culture enhance expression of *Cyp26b1*, which was shown by others to represent a RA hydroxylase.[66] Co-culture in the presence of the ALDH1A2 inhibitor WIN18,446 reduced the expression of ICO marker *Gpc3,* and addition of RA to mono-cultured ICOs did increase expression of both *Gpc3* and *Mmp7*. This indicates that RA production can be responsible for some of the effects of co-culture seen on gene expression in ICOs. Unfortunately, attempts to measure RA production in cultured HSCs and in the medium by mass spectrometry were unsuccessful, most likely due to the combination of low cell numbers, low RA concentrations as a signaling molecule, and its chemical instability.[67]

The upregulation of frizzled binding/Wnt-related genes (including *Wnt5a* and *Wnt11*) was also specific for co-

cultured HSCs as compared with other HSCs and suggests that Wnt signaling is active in co-cultured HSCs. Upregulation of Wnt signaling has been described during liver damage/regeneration and fibrosis and in activating HSCs both *in vitro* and *in vivo*.[68–71] ICOs also exhibit active Wnt signaling under proliferating conditions,[10] and, both in mono- and co-cultured ICOs, *Wnt7b* and *Wnt7a* are highly expressed (data not shown). In agreement with this, active Wnt signaling is also seen *in vivo* in a Cd44-positive population of biliary epithelial cells after DDC treatment in mice,[72] and after BDL in mice and rats.[73] Consistent with (additional) Wnt secretion in co-culture, expression of *Cthrc1* and *Aldh1a2* (in co-cultured HSCs) and *Mmp7* (in co-cultured ICOs) was increased. Expression of *Cthrc1*, *Aldh1a2,* and *Mmp7* can all be regulated by Wnt signaling.[74–76] CTHRC1 has been described to induce Wnt signaling in different cell types.[62,77] *Gpc3*, which is also upregulated in co-cultured ICOs, has been found to be able to enhance Wnt signaling by serving as a co-receptor for Wnt.[50] Several studies observed a role for Wnt5a and non-canonical Wnt signaling in liver damage and fibrosis.[48,69–71] Inhibition of Wnt signaling has been found to reduce fibrosis formation,[48,70] although another study found that elimination of Wnt specifically in HSCs had no effect on proliferation or fibrosis formation,[78] and Wilson et al suggested that macrophages are the source of Wnt5a instead of fibroblasts.[48] Our co-culture model does, however, suggest that Wnt signaling plays a role in the interaction between ICOs and HSCs. A possible scenario could be that baseline levels of Wnt (Wnt7) from ICOs influence HSCs to increase some of the co-culture specific genes such as *Aldh1a2* and *Cthrc1*. In turn, HSCs become activated and produce RA and other Wnts (5 and/or 11). Wnt5a and Wnt-11 and Rho/Rho kinase/c-Jun $NH_2$-terminal kinase are associated with the noncanonical Wnt pathway.[79] The strong inhibitory effects of the Wnt inhibitor SP600125 (an inhibitor of JNK) may suggest that non-canonical Wnt signaling is involved in the HSC interaction with ICOs, thereby enhancing proliferation and *Mmp7* expression through Wnt and increasing expression of *Gpc3* via RA in ICOs. Enhanced *Gpc3* expression in the ICOs and enhanced *Cthrc1* expression in the HSCs then further enhances Wnt signaling (Figure 8*E*).

In conclusion, the HSC-ICO 3D co-culture system provides a novel approach to elucidate the interactions between ductular reactions and fibrosis in liver diseases that are relevant for human liver diseases. Ductular reactions in the liver can be triggered by various etiologies and play an important role in the fibrogenesis of various liver diseases, including biliary atresia, MASLD, genetic cholestatic diseases (eg, progressive familial intrahepatic cholestasis), and cholestatic cholangiopathies (eg, PBC and PSC).[3,46,47] Our transcriptomics analysis and functional characterization support that the HSC-ICO 3D co-culture model can be adapted to model liver diseases characterized by persistent ductular reaction and progressive fibrosis. By using donor-matched ICOs and HSCs from patients with liver disease[80,81] or their corresponding murine models, the present HSC-ICO 3D co-culture platform provides unique opportunities to dissect etiology-specific interactions between the HSCs and the hepatic progenitor cells and to obtain new insight in developing new anti-fibrotic therapies for liver diseases.

# Methods

## Murine HSC Isolation

HSCs were isolated from healthy wild-type BALB/c mice that were minimally 3 months old. Typically, cells from multiple mice were pooled per experiment, containing both male and female mice. The isolation protocol of Mederacke et al was used.[82] In short, livers were perfused with pronase and collagenase solutions, after which HSCs were separated from other cells by Nycodenz gradient centrifugation. The purity of isolated HSCs was confirmed by determining the percentage of UV positive (due to the presence of retinyl-esters in lipid droplets) HSCs. HSCs were routinely obtained with >96% to 98% purity. Mice experiments were approved by the Dutch Animal Experimental Licensing Committee (DEC) (DEC number: AVD1080020174484).

## Cell Culture

HSCs were plated on plastic (2D culture) or embedded in a droplet of growth factor reduced Matrigel (Corning) (3D culture). ICOs were isolated from mT/mG mice (tissue material provided by the lab of Prof Dr N. Geijsen), which express the fluorescent membrane-targeted protein tandem dimer Tomato (tdTomato). ICOs were isolated and expanded in culture as described[10] in expansion medium (EM) containing AdDMEM/F12 (Invitrogen) supplemented with B27 and N2 (Invitrogen), N-Acetylcysteine (1.25 $\mu$M, Sigma), gastrin (10 nM, Sigma), EGF (50 ng/mL, Peprotech), FGF10 (100 ng/mL, Peprotech), nicotinamide (10 mM, Sigma), and HGF (50 ng/mL, Peprotech), with the only difference being the replacement of RSPO1 conditioned medium for RSPO3 (2% (v/v), ImmunoPrecise Antibodies). Primary HSCs cultured in Matrigel with 100% EM were not viable. A mixture of 50% EM and 50% of the regular HSC culture medium (DMEM with 10% [v/v] FBS) was suitable for our co-culture experiments, and all experiments were performed in this medium (termed co-culture medium), including mono-culture controls. Medium was replaced every 3 days. ICOs were used at passage number 8-20. Before co-culture, ICOs were fragmented and mixed with similar amounts of freshly isolated HSCs. Mono-cultures and co-cultures were started with similar amounts of total cells (ie, one-half of the amount of each cell type that was used in mono-culture was used in co-cultures). Cells were cultured in 24 wells, 48 wells, or microscopy plates, depending on the read-out. For a 24-well, a total amount of 100,000 cells/well were plated in droplets of 50 $\mu$L Matrigel with 500 $\mu$L medium. For co-culture in separate droplets, 25 $\mu$L of Matrigel with HSCs and 25 $\mu$L of Matrigel with ICOs was plated in the same well. Bright field images of cultures were taken with a CKX53 inverted microscope (Olympus Nederland B.V.). In some cell culture experiments, the following materials and chemicals were used: Mouse TGF$\beta$1 recombinant protein was purchased at ThermoFisher Scientific, all-trans-RA at Sigma Aldrich, C59 (Wnt inhibitor) at Abcam,

and WIN18,446 (ALDH1A2 inhibitor), ICG-001, LF-3 and SP600125 at Sanbio B.V.

## Sandwich Enzyme-linked Immunosorbent Assay for Murine Pro-collagen 1A1

The secretion of type I collagen protein was determined by measuring the medium concentration of procollagen type I N-terminal propeptide (PINP), which is cleaved off the type I collagen fiber during maturation. The capture and detection antibody pair for the N-terminal peptide of pro-collagen 1A1 was obtained from Abcam (AB216791). The 96-well high binding enzyme-linked immunosorbent assay (ELISA) microplate (R&D Systems DY990) was coated with 50 $\mu$L 2 $\mu$g/mL capture antibody in sterilized 50 mM $NaHCO_3$-$Na_2CO_3$ buffer (pH 9.6) overnight at 4 °C. The unbound capture antibody was washed away with phosphate-buffered saline with Tween (PBST) and the plate was blocked with 1% (w/v) bovine serum albumin (BSA) in phosphate buffered saline (PBS) (BSA/PBS) for 1 hour at room temperature. All subsequent incubation steps were preceded by three wash steps with PBST and performed at room temperature. After removing the blocking solution, 50-$\mu$L samples (diluted 10–100 times with BSA/PBS) and standards (31.5 to 2000 pg/mL in BSA/PBS) were added to the well and incubated for 2 hours, followed by incubation with 50-$\mu$L 0.5 $\mu$g/mL biotinylated detection antibody in BSA/PBS for 2 hours, and 1× streptavidin-HRP solution (R&D Systems DY999). The signal was developed with 100-$\mu$L tetramethylbenzidine solution (R&D Systems DY999) and stopped with 50-$\mu$L 1 M $H_2SO_4$. The absorbance was measured with the spectrophotometer SPECTROstar (BMG Labtech) at 450 nm with the reference wavelength at 570 nm. Concentration of PINP was calculated based on the standard curve by 4-parameter logistic regression.

## Metabolic Activity

Metabolic activity as a measure for viable cell amounts was determined with Cell Counting Kit-8 (Sigma) which uses WST-8 (2-(2-methoxy-4-nitrophenyl)-3-(4-nitrophenyl)-5-(2,4-disulfophenyl)-2H-tetrazolium), a tetrazolium salt. Assay was performed according to manufacturer's protocol and analysis of the color change of the medium was analyzed by absorbance at 450 nm using a spectrophotometer SPECTROstar (BMG Labtech). The 'expected signal' in 3D co-culture represents the expected metabolic activity when no interaction between different cell types takes place. Because one-half of the amount of each cell type that was used in mono-culture was used in co-cultures, it is defined as 0.5× (the metabolic activity of ICO 3D mono-culture + the metabolic activity of HSC 3D mono-culture).

## FACS

After 7 days of culture, Matrigel was removed with cold PBS and digested to single cells using trypsin for 15 minutes at 37 °C. Cell sorting was performed at the Flow Cytometry and Cell Sorting Facility of the Faculty of Veterinary Medicine at Utrecht University. Cells were sorted using a BD Influx cell sorter (BD Bioscience, San Jose, CA), equipped with BD Spigot software version 6.1. tdTomato was laser excited at 561 nm, and fluorescence was detected at 585 nm using a 42-band pass filter. In every experimental setting, the same detector settings and sort gates were used; no scatter gate was included. Cells were solely sorted on tdTomato positive and tdTomato negative. Cells were sorted in PBS with 2% (v/v) FBS. PBS served as sheath fluid.

## Confocal Microscopy

Cells were grown on CELLView slides (Greiner Bio-One BV) and kept in the dark until imaging. Images were taken without prior fixation with a Leica TCSSPE-II confocal microscope (Leica Microsystems) at the Center of Cellular Imaging (Faculty of Veterinary Medicine, Utrecht University, The Netherlands). Auto-fluorescence of retinoids was imaged by 405 nm laser excitation; the emission was detected between 415 and 450 nm.

## RNA Isolation and rt-qPCR

RNA was isolated using a RNeasy Micro Kit (Qiagen) including an on-column DNase-I treatment to minimize DNA contamination. cDNA was synthesized using an iScript cDNA Synthesis Kit (Bio-Rad). The PCR amplifications were performed using a Bio-Rad detection system with iQ SYBR Green Supermix (Bio-Rad). A 4-fold dilution series from a pool of the samples was used to determine relative gene expression levels normalized to the average levels of reference genes. Reference genes, primer sequences, and annealing temperatures are listed in Supplementary Table 1.

## RNA Sequencing: Library Preparation and Sequencing

The libraries were prepared following the protocol for Smart-seq2.[83] Following reverse transcription, an Agilent 4200 TapeStation System was used to evaluate the quality of the cDNAs. Using an Illumina Nextera XT kit, 1.0 ng of amplified cDNA from each sample was tagmented and amplified. The resulting libraries were pooled, double-sided size selected (0.5× followed by 0.8× ratio using Beckman Ampure XP beads), and quantified using an Agilent 4200 TapeStation System. The pool of libraries was sequenced with a depth of around 20 Mio reads per sample in an Illumina NovaSeq6000 sequencer (single-end 100 bp).

## RNA Sequencing: Data Analysis

The RNA sequencing data analysis consisted of the following steps: The raw reads were first cleaned by removing adapter sequences and poly-x sequences (>9 nt used for detection) using fastp (Version 0.20.0).[84] Sequence pseudo alignment of the resulting high-quality reads to the Mouse reference genome (build GRCm39) and quantification of gene-level expression (gene model definition from GENCODE release M26) was carried out using Kallisto (Version 0.46.1).[85] To detect DEGs, we used the glm approach implemented in the software package DESeq2 (R version: 4.2.0, DESeq2 version: 1.36.0).[86] Genes showing

altered expression with *P*-value $\leq$ .01 and log2 ratio $\geq$ 0.5 were considered significant. Over-representation analysis (ORA) was conducted based on DEGs with *P*-value $<$ .01 and log2 ratio $>$1 using clusterProfiler (Version 4.4.4).[87] Terms with a false discovery rate $<$.05 were considered significant. The Multi-DEG app of the Functional Genomics Center Zurich was used to check for overlaps in DEGs and ontology terms between the 2-group DE analyses. Data is available via the Gene Expression Omnibus, accession number: GSE264276.

### Human Liver Samples, Ethics, and Consent

End-stage liver biopsies (n = 8) from patients with PSC (n = 4), PBC (n = 2), and alcohol-related liver disease (n = 2) were collected following liver transplantation.[41] Written informed consent was obtained from all study participants, and study ethics were approved by regional Committees for Medical and Health Research Ethics of South East Norway (reference numbers: 2012-286 and 2016-1540) in accordance with the Declaration of Helsinki.

### Spatial Transcriptomics and Bioinformatics

Spatial transcriptomics assessment of the samples has been previously described.[41] Briefly, cryopreserved liver samples sectioned at 10 $\mu$m were permeabilized for 25 minutes and analyzed on RNA capture slides (Visium, 10$\times$ Genomics) following the manufacturer's protocol (User guide CG000239 Rev D, 10$\times$ Genomics). Sequencing reads were demultiplexed and aligned to the human genome (GRCh39) using Space Ranger (v.1.1.0, 10$\times$ Genomics) and visualized using Loupe Browser (v.7.0.1, 10$\times$ Genomics).

Spatial transcriptomes were analyzed in RStudio using Seurat v.5.0.5.[88] Pre-processed data was normalized and variable features were defined using SCTransform v.0.4.1.[89] PCA of variable features was computed using the Seurat RunPCA function and integrated to correct for batch and technical artifacts using Harmony v.1.2.0.[90] Dimensionality reduction was performed by neighbor graph-based clustering using the Seurat RunUMAP function set to 20 principal components, and cluster numbers were adjusted using the resolution parameter of the Seurat FindClusters function set between 0.05 to 4. Stable clusters were defined by at least 10 DEGs of significance ($P < .05$) detected at greater than one average count per spot. DEGs of statistical significance were calculated in Loupe Browser v.7.0.1 (10$\times$ Genomics) using the exact negative binomial test and Benjamini-Hochberg corrected for multiple testing. All standard statistical analyses were performed using Prism v.10.2.2 (GraphPad) unless otherwise stated. *P*-values for comparative analysis of positive spots within the parenchyma and fibrosis were calculated using parametric 2-tailed unpaired Student *t*-test. R-values and *P*-values from correlation analysis of indicated gene expression were calculated using 2-tailed nonparametric Spearman analysis.

### Image Design and Statistics

Bar plots were generated using GraphPad Prism version 9.3.1, using either a 1-sample *t*-test, Welch *t*-test, Mann-Whitney test, 1-way or a 2-way analysis of variance (ANOVA) with a Šídák's multiple comparisons correction for statistics. For (overview) image design, Adobe Illustrator 2023 was used.

## Supplementary Material

Note: To access the supplementary material accompanying this article, visit the full text version of *Cellular and Molecular Gastroenterology and Hepatology* at https://doi.org/10.1016/j.jcmgh.2025.101472.

## References


1. Asrani SK, Devarbhavi H, Eaton J, Kamath PS. Burden of liver diseases in the world. J Hepatol 2019;70:151–171.
2. Rinella ME, Lazarus JV, Ratziu V, et al, NAFLD Nomenclature consensus group. A multi-society Delphi consensus statement on new fatty liver disease nomenclature. Ann Hepatol 2024;29:101133.
3. Sato K, Marzioni M, Meng F, et al. Ductular reaction in liver diseases: pathological mechanisms and translational significances. Hepatology 2019;69:420–430.
4. Chen Y, Gao WK, Shu YY, Ye J. Mechanisms of ductular reaction in non-alcoholic steatohepatitis. World J Gastroenterol 2022;28:2088–2099.
5. Roskams TA, Theise ND, Balabaud C, et al. Nomenclature of the finer branches of the biliary tree: canals, ductules, and ductular reactions in human livers. Hepatology 2004;39:1739–1745.
6. Marsee A, Roos FJM, Verstegen MMA, et al. Building consensus on definition and nomenclature of hepatic, pancreatic, and biliary organoids. Cell Stem Cell 2021;28:816–832.
7. Babboni S, Vacca PG, Simonini L, et al. Cholangiocyte organoids: the new frontier in regenerative medicine for the study and treatment of cholangiopathies. J Clin Med 2024;13:1804.
8. Verstegen MMA, Roos FJM, Burka K, et al. Human extrahepatic and intrahepatic cholangiocyte organoids show region-specific differentiation potential and model cystic fibrosis-related bile duct disease. Sci Rep 2020;10:21900.
9. Sampaziotis F, Justin A, Tysoe O, et al. Reconstruction of the mouse extrahepatic biliary tree using primary human extrahepatic cholangiocyte organoids. Nat Med 2017:954–963.
10. Huch M, Dorrell C, Boj SF, et al. In vitro expansion of single Lgr5 + liver stem cells induced by Wnt-driven regeneration. Nature 2013;494:247–250.
11. Aloia L, McKie MA, Vernaz G, et al. Epigenetic remodelling licences adult cholangiocytes for organoid formation and liver regeneration. Nat Cell Biol 2019;21:1321–1333.
12. de Lau W, Peng WC, Gros P, Clevers H. The R-spondin/Lgr5/Rnf43 module: regulator of Wnt signal strength. Genes Dev 2014;28:305–316.
13. Wang Z, Xing C, van der Laan LJW, et al. Cholangiocyte organoids to study drug-induced injury. Stem Cell Res Ther 2024;15:78.

14. Broutier L, Andersson-Rolf A, Hindley CJ, et al. Culture and establishment of self-renewing human and mouse adult liver and pancreas 3D organoids and their genetic manipulation. Nat Protoc 2016;11:1724–1743.
15. Zhao L, Westerhoff M, Pai RK, et al. Centrilobular ductular reaction correlates with fibrosis stage and fibrosis progression in non-alcoholic steatohepatitis. Mod Pathol 2018;31:150–159.
16. Rókusz A, Veres D, Szücs A, et al. Ductular reaction correlates with fibrogenesis but does not contribute to liver regeneration in experimental fibrosis models. PLoS One 2017;12:e0176518.
17. O'Rourke JM, Sagar VM, Shah T, Shetty S. Carcinogenesis on the background of liver fibrosis: implications for the management of hepatocellular cancer. World J Gastroenterol 2018;24:4436–4447.
18. Mederacke I, Hsu CC, Troeger JS, et al. Fate-tracing reveals hepatic stellate cells as dominant contributors to liver fibrosis independent of its etiology. Nat Commun 2013;4:2823.
19. Haaker MW, Vaandrager AB, Helms JB. Retinoids in health and disease: a role for hepatic stellate cells in affecting retinoid levels. Biochim Biophys Acta Mol Cell Biol Lipids 2020;1865:158764.
20. Tsuchida T, Friedman SL. Mechanisms of hepatic stellate cell activation. Nat Rev Gastroenterol Hepatol 2017;14:397–411.
21. De Minicis S, Seki E, Uchinami H, et al. Gene expression profiles during hepatic stellate cell activation in culture and in vivo. Gastroenterology 2007;132:1937–1946.
22. Dobie R, Wilson-Kanamori JR, Henderson BEP, et al. Single-cell transcriptomics uncovers zonation of function in the mesenchyme during liver fibrosis. Cell Rep 2019;29:1832–1847.e8.
23. Rosenthal SB, Liu X, Ganguly S, et al. Heterogeneity of HSCs in a mouse model of NASH. Hepatology 2021;74:667–685.
24. Clouston AD, Jonsson JR, Powell EE. Hepatic progenitor cell-mediated regeneration and fibrosis: chicken or egg? Hepatology 2009;49:1424–1426.
25. Williams MJ, Clouston AD, Forbes SJ. Links between hepatic fibrosis, ductular reaction, and progenitor cell expansion. Gastroenterology 2014;146:349–356.
26. Van Hul NKM, Abarca-Quinones J, Sempoux C, et al. Relation between liver progenitor cell expansion and extracellular matrix deposition in a CDE-induced murine model of chronic liver injury. Hepatology 2009;49:1625–1635.
27. Pintilie DG, Shupe TD, Oh SH, et al. Hepatic stellate cells involvement in progenitor mediated liver regeneration. Lab Invest 2011;90:1199–1208.
28. Zhang Z, Zhong X, Shen H, et al. Biliary NIK promotes ductular reaction and liver injury and fibrosis in mice. Nat Commun 2022;13:5111.
29. Friedman SL, Roll FJ, Boyles J, et al. Maintenance of differentiated phenotype of cultured rat hepatic lipocytes by basement membrane matrix. J Biol Chem 1989;264:10756–10762.
30. Haaker MW, Goossens V, Hoogland NAN, et al. Early activation of hepatic stellate cells induces rapid initiation of retinyl ester breakdown while maintaining lechthin: retinol acyltrasnferase (LRAT) activity. Biochim Biophys Acta Mol Cell Biol Lipids 2024;1869:159540.
31. Wells RG. The role of matrix stiffness in hepatic stellate cell activation and liver fibrosis. J Clin Gastroenterol 2005;39(Suppl 2):S158–S161.
32. Shmarakov IO, Jiang H, Liu J, et al. Hepatic stellate cell activation: a source for bioactive lipids. Biochim Biophys Acta Mol Cell Biol Lipids 2019;1864:629–642.
33. Chiu CC, Sheu JC, Chen CH, et al. Global gene expression profiling reveals a key role of CD44 in hepatic oval-cell reaction after 2-AAF/CCl4 injury in rodents. Histochem Cell Biol 2009;132:479–489.
34. Grozdanov PN, Yovchev MI, Dabeva MD. The oncofetal protein glypican-3 is a novel marker of hepatic progenitor/oval cells. Lab Invest 2006;86:1272–1284.
35. Zheng X, Liu X, Lei Y, et al. Glypican-3: a novel and promising target for the treatment of hepatocellular carcinoma. Front Oncol 2022;12:824208.
36. Lee YS, Jeong W Il. Retinoic acids and hepatic stellate cells in liver disease. J Gastroenterol Hepatol 2012;27-(Suppl 2):75–79.
37. Proffitt KD, Madan B, Ke Z, et al. Pharmacological inhibition of the Wnt acyltransferase PORCN prevents growth of WNT-driven mammary cancer. Cancer Res 2013;73:502–507.
38. Emami KH, Nguyen C, Ma H, et al. A small molecule inhibitor of $\beta$-catenin/cyclic AMP response element-binding protein transcription. Proc Natl Acad Sci U S A 2004;101:12682–12687.
39. Fang L, Zhu Q, Neuenschwander M, et al. A small-molecule antagonist of the $\beta$-catenin/TCF4 interaction blocks the self-renewal of cancer stem cells and suppresses tumorigenesis. Cancer Res 2016;76:891–901.
40. Bennett BL, Sasaki DT, Murray BW, et al. SP600125, an anthrapyrazolone inhibitor of Jun N-terminal kinase. Proc Natl Acad Sci U S A 2001;98:13681–13686.
41. Chung BK, Øgaard J, Reims HM, et al. Spatial transcriptomics identifies enriched gene expression and cell types in human liver fibrosis. Hepatol Commun 2022;6:2538–2550.
42. Boulter L, Govaere O, Bird T, et al. Macrophage derived Wnt signalling opposes Notch signalling in a Numb mediated manner to specify HPC fate in chronic liver disease in human and mouse. Nat Med 2012;18:572–579.
43. Iwaisako K, Jiang C, Zhang M, et al. Origin of myofibroblasts in the fibrotic liver in mice. Proc Natl Acad Sci U S A 2014;111:E3297–E3305.
44. Lua I, Li Y, Zagory JA, et al. Characterization of hepatic stellate cells, portal fibroblasts, and mesothelial cells in normal and fibrotic livers. J Hepatol 2016;64:1137–1146.
45. Irvine KM, Okano S, Patel PJ, et al. Serum matrix metalloproteinase 7 (MMP7) is a biomarker of fibrosis in patients with non-alcoholic fatty liver disease. Sci Rep 2021;11:2858.
46. Nomden M, Beljaars L, Verkade HJ, et al. Current concepts of biliary atresia and matrix metalloproteinase-7: a review of literature. Front Med 2020;7:617261.

47. Kerola A, Lampela H, Lohi J, et al. Increased MMP-7 expression in biliary epithelium and serum underpins native liver fibrosis after successful portoenterostomy in biliary atresia. J Pathol Clin Res 2016;2:187–198.
48. Wilson DH, Jarman EJ, Mellin RP, et al. Non-canonical Wnt signalling regulates scarring in biliary disease via the planar cell polarity receptors. Nat Commun 2020; 11:445.
49. Sun CK, Chua MS, He J, So SK. Suppression of glypican 3 inhibits growth of hepatocellular carcinoma cells through up-regulation of TGF-$\beta$2. Neoplasia 2011; 13:735–747.
50. Kolluri A, Ho M. The role of glypican-3 in regulating Wnt, YAP, and hedgehog in liver cancer. Front Oncol 2019; 9:708.
51. Xia L, Teng Q, Chen Q, Zhang F. Preparation and characterization of anti-GPC3 nanobody against hepatocellular carcinoma. Int J Nanomedicine 2020;15:2197–2205.
52. Liao HY, Da CM, Liao B, Zhang HH. Roles of matrix metalloproteinase-7 (MMP-7) in cancer. Clin Biochem 2021;92:9–18.
53. Lin Y, Liu J, Huang Y, et al. microRNA-489 plays an anti-metastatic role in human hepatocellular carcinoma by targeting matrix metalloproteinase-7. Transl Oncol 2017; 10:211–220.
54. Breitkopf-Heinlein K, Meyer C, König C, et al. BMP-9 interferes with liver regeneration and promotes liver fibrosis. Gut 2017;66:939–954.
55. Addante A, Roncero C, Almalé L, et al. Bone morphogenetic protein 9 as a key regulator of liver progenitor cells in DDC-induced cholestatic liver injury. Liver Int 2018;38:1664–1675.
56. Chen L, Zhou T, White T, et al. The apelin–apelin receptor axis triggers cholangiocyte proliferation and liver fibrosis during mouse models of cholestasis. Hepatology 2021; 73:2411–2428.
57. Murphy G, Cockett MI, Ward RV, Docherty AJP. Matrix metalloproteinase degradation of elastin, type IV collagen and proteoglycan: a quantitative comparison of the activities of 95 kDa and 72 kDa gelatinases, stromelysins-1 and -2 and punctuated metalloproteinase (PUMP). Biochem J 1991;277:277–279.
58. Wang FQ, So J, Reierstad S, Fishman DA. Matrilysin (MMP-7) promotes invasion of ovarian cancer cells by activation of progelatinase. Int J Cancer 2005; 114:19–31.
59. Balazova L, Balaz M, Horvath C, et al. GPR180 is a component of TGF$\beta$ signalling that promotes thermogenic adipocyte function and mediates the metabolic effects of the adipocyte-secreted factor CTHRC1. Nat Commun 2021;12:7144.
60. Ruiz-Villalba A, Romero J, Hernández S, et al. Single-cell RNA sequencing analysis reveals a crucial role for CTHRC1 (Collagen Triple Helix Repeat Containing 1) cardiac fibroblasts after myocardial infarction. Circulation 2020;142:1831–1847.
61. Tsukui T, Sun KH, Wetter JB, et al. Collagen-producing lung cell atlas identifies multiple subsets with distinct localization and relevance to fibrosis. Nat Commun 2020; 11:1920.
62. Li J, Wang Y, Ma M, et al. Autocrine CTHRC1 activates hepatic stellate cells and promotes liver fibrosis by activating TGF-$\beta$ signaling. EBioMedicine 2019; 40:43–55.
63. Blaner WS, Li Y, Brun P, et al. Vitamin A absorption, storage and mobilization. Subcell Biochem 2016;81:95–125.
64. Testerink N, Ajat M, Houweling M, et al. Replacement of retinyl esters by polyunsaturated triacylglycerol species in lipid droplets of hepatic stellate cells during activation. PLoS One 2012;7:e34945.
65. Shmarakov IO, Jiang H, Yang KJZ, et al. Hepatic retinoid stores are required for normal liver regeneration. J Lipid Res 2013;54:893–908.
66. Topletz AR, Thatcher JE, Zelter A, et al. Comparison of the function and expression of CYP26A1 and CYP26B1, the two retinoic acid hydroxylases. Biochem Pharmacol 2012;83:149–163.
67. Al Tanoury Z, Piskunov A, Rochette-Egly C. Vitamin A and retinoid signaling: genomic and nongenomic effects. J Lipid Res 2013;54:1761–1775.
68. Corbett L, Mann J, Mann DA. Non-canonical Wnt predominates in activated rat hepatic stellate cells, influencing Hsc survival and paracrine stimulation of Kupffer cells. PLoS One 2015;10:e0142794.
69. Beljaars L, Daliri S, Dijkhuizen C, et al. WNT-5A regulates TGF-$\beta$-related activities in liver fibrosis. Am J Physiol Gastrointest Liver Physiol 2017;312:G219–G227.
70. Cheng JH, She H, Han YP, et al. Wnt antagonism inhibits hepatic stellate cell activation and liver fibrosis. Am J Physiol Gastrointest Liver Physiol 2007; 294:G39–G49.
71. Jiang F, Parsons CJ, Stefanovic B. Gene expression profile of quiescent and activated rat hepatic stellate cells implicates Wnt signaling pathway in activation. J Hepatol 2006;45:401–409.
72. Pepe-Mooney BJ, Dill MT, Alemany A, et al. Single-cell analysis of the liver epithelium reveals dynamic heterogeneity and an essential role for YAP in homeostasis and regeneration. Cell Stem Cell 2019;25:23–38.e8.
73. Okabe H, Yang J, Sylakowski K, et al. Wnt signaling regulates hepatobiliary repair following cholestatic liver injury in mice. Hepatology 2016;64:1652–1666.
74. Liu G, Sengupta PK, Jamal B, et al. N-glycosylation induces the CTHRC1 protein and drives oral cancer cell migration. J Biol Chem 2013;288:20217–20227.
75. Mathew LK, Sengupta S, Franzosa JA, et al. Comparative expression profiling reveals an essential role for Raldh2 in epimorphic regeneration. J Biol Chem 2009; 284:33642–33653.
76. Brabletz T, Jung A, Dag S, et al. B-catenin regulates the expression of the matrix metalloproteinase-7 in human colorectal cancer. Am J Pathol 1999;155:1033–1038.
77. Mei D, Zhu Y, Zhang L, Wei W. The role of CTHRC1 in regulation of multiple signaling and tumor progression and metastasis. Mediators Inflamm 2020;2020: 9578701.
78. Zhang R, Kikuchi AT, Nakao T, et al. Elimination of Wnt secretion from stellate cells is dispensable for zonation and development of liver fibrosis following hepatobiliary injury. Gene Expr 2019;19:121–136.

79. Seifert JRK, Mlodzik M. Frizzled/PCP signalling: a conserved mechanism regulating cell polarity and directed motility. Nat Rev Genet 2007;8:126–138.
80. Shang L, Hosseini M, Liu X, et al. Human hepatic stellate cell isolation and characterization. J Gastroenterol 2018; 53:6–17.
81. Huch M, Gehart H, Van Boxtel R, et al. Long-term culture of genome-stable bipotent stem cells from adult human liver. Cell 2015;160:299–312.
82. Mederacke I, Dapito DH, Affò S, et al. High-yield and high-purity isolation of hepatic stellate cells from normal and fibrotic mouse livers. Nat Protoc 2015;10:305–315.
83. Picelli S, Faridani OR, Björklund ÅK, et al. Full-length RNA-seq from single cells using Smart-seq2. Nat Protoc 2014;9:171–181.
84. Chen S, Zhou Y, Chen Y, Gu J. Fastp: an ultra-fast all-in-one FASTQ preprocessor. Bioinformatics 2018;34:i884–i890.
85. Bray N, Pimentel H, Melsted P, Pachter L. Near-optimal probabilistic RNA-seq quantification. Nat Biotechnol 2016;34:525–527.
86. Love MI, Huber W, Anders S. Moderated estimation of fold change and dispersion for RNA-seq data with DESeq2. Genome Biol 2014;15:550.
87. Wu T, Hu E, Xu S, et al. clusterProfiler 4.0: a universal enrichment tool for interpreting omics data. Innovation (Camb) 2021;2:100141.
88. Hao Y, Stuart T, Kowalski M, et al. Dictionary learning for integrative, multimodal, and massively scalable single-cell analysis. Nat Biotechnol 2024;42:293–304.
89. Hafemeister C, Satija R. Normalization and variance stabilization of single-cell RNA-seq data using regularized negative binomial regression. Genome Biol 2019;20:296.
90. Korsunsky I, Millard N, Fan J, et al. Fast, sensitive, and accurate integration of single cell data with Harmony. Nat Methods 2019;16:1289–1296.

**Received April 25, 2024. Accepted January 23, 2025.**

**Correspondence**
Address correspondence to: J. Bernd Helms, Department of Biomolecular Health Sciences, Faculty of Veterinary Medicine, Utrecht University, The Netherlands, Yalelaan 2, 3584 CM Utrecht, Netherlands. e-mail: j.b.helms@uu.nl.

**Acknowledgments**
The authors thank Ger Arkesteijn for sorting of the cells, Richard Wubbolts for help optimizing the settings of the confocal microscope, and Adam Myszczyszyn for his critical comments and discussion.

**CRediT Authorship Contributions**
Maya W. Haaker (Data curation: Lead; Formal analysis: Lead; Investigation: Lead; Methodology: Equal; Visualization: Lead; Writing – original draft: Lead)
Jung-Chin Chang (Investigation: Supporting; Methodology: Equal; Writing – review & editing: Supporting)
Brian K. Chung (Data curation: Equal; Methodology: Equal; Visualization: Equal; Writing – review & editing: Equal)
Tobias S. Pieper (Investigation: Supporting)
Falko Noé (Data curation: Supporting; Formal analysis: Supporting; Methodology: Supporting)
Tongtong Wang (Formal analysis: Supporting; Methodology: Supporting)
Niels Geijsen (Resources: Supporting; Writing – review & editing: Supporting)
Martin Houweling (Investigation: Supporting; Methodology: Supporting; Project administration: Equal)
Christian Wolfrum (Resources: Supporting; Writing – review & editing: Supporting)
Arie B. Vaandrager (Conceptualization: Equal; Supervision: Equal; Writing – review & editing: Equal)
Espen Melum (Methodology: Equal; Writing – review & editing: Equal)
Bart Spee (Conceptualization: Equal; Writing – review & editing: Supporting)
J. Bernd Helms (Conceptualization: Lead; Project administration: Lead; Supervision: Lead; Writing – review & editing: Lead)

**Conflicts of interest**
The authors disclose no conflicts.